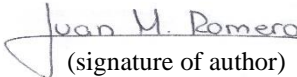




Universitetet  
i Stavanger

**FACULTY OF SCIENCE AND TECHNOLOGY**

# **MASTER'S THESIS**

Study programme/specialisation: Petroleum Engineering / Well Engineering	Spring semester, 2020  Open
Author: Juan Manuel Romero Rubio	 (signature of author)
Supervisor(s): Jan Aage Aasen	
Title of master's thesis: Compatibility between API equations and design limits plots for ellipse and circle of plasticity	
Credits: 30 ETCS	
Keywords: Pipe collapse API 5C3 Ellipse of plasticity Circle of plasticity Design limits plot	Number of pages: 81  + supplemental material/other: .....  Stavanger, July 1 <sup>st</sup> , 2020 date/year

# Acknowledgements

Thanks to my mother, Neila, and my uncle, Marco, who supported me to come to Norway. Without them, this project would have never become real. Thanks to my supervisor, Jan, who was always available to answer my questions, give me advice, and encourage me to analyze problems deeper to find solutions.

# Abstract

This project presents a methodology to superimpose the API uniaxial and triaxial limits on the design limits plot. Complications due to a recent change of axis are resolved, producing practical design limits plots that avoid the horizontal shift of the API vertical limits, currently done by the industry. The commonly used slanted ellipse is compared against an adaptation of the circle of plasticity in the form of a horizontal ellipse, showing the convenience of this last one with examples.

After a new collapse formulation was introduced in API TR 5C3 in 2015, the horizontal axis on the standard industry well tubular design limits plot changed. The study evaluates this redefinition of the horizontal axis. One consequence of this modification is a difficulty plotting the API tension and compression limits. The API horizontal limits (uniaxial burst and collapse) are found to be independent of load case, while the API vertical design limits (uniaxial tension and compression) are dependent on inside and outside tubular pressures. The approaches used by commercial software and industry publications to solve this challenge are analyzed. A new design methodology is developed to link API limits to the triaxial theory.

The main objective of the study is to establish a mathematical relationship between API tubular design limits and the Von Mises triaxial theory. A methodology that allows plotting the API uniaxial force limits on the design limit plot is developed. The study also shows that the results obtained from the industry standard slanted ellipse are identical to those obtained from the horizontal ellipse/circle and therefore the new plotting methodology can be applied to the last one as well. A difference is that the slanted ellipse is based on zero axial stress datum while the horizontal ellipse/circle uses neutral axial stress datum. The horizontal ellipse/circle is well suited for calculations involving buckling, is compatible with the information used in field operations, and its formulations are less complicated than in the tilted ellipse, therefore attention is called to it.

# Contents

<b>1</b>	<b>Introduction</b>	<b>1</b>
<b>2</b>	<b>Theory</b>	<b>3</b>
2.1	Casing and tubing . . . . .	3
2.2	Stress analysis in casing and tubing . . . . .	5
2.2.1	Cylinders types and stress calculations . . . . .	6
2.2.2	Yield strength . . . . .	7
2.2.3	Burst pressure . . . . .	8
2.2.4	Collapse pressure . . . . .	8
2.2.5	Triaxial loads . . . . .	11
2.2.6	Critical dimensions . . . . .	11
2.3	Effective force . . . . .	12
2.4	Yield circle and ellipse . . . . .	13
2.5	History of API collapse equation . . . . .	15
<b>3</b>	<b>Method</b>	<b>18</b>
3.1	Comparison of previous and new API equation . . . . .	18
3.2	API equations and design limits plots . . . . .	19
3.3	Implementation of the circle of plasticity . . . . .	21

3.4	API collapse equation in neutral stress datum . . . . .	21
<b>4</b>	<b>Results and discussion</b>	<b>22</b>
4.1	Discussion of new API equation . . . . .	22
4.2	Evaluation of current industry approaches to plot API limits . . . . .	24
4.2.1	Goodman et al. . . . .	24
4.2.2	Commercial software approach . . . . .	26
4.3	Evaluation of new approaches . . . . .	31
4.3.1	Separated plots . . . . .	31
4.3.2	Slanted line . . . . .	33
4.3.3	Color scheme . . . . .	35
4.4	Implementation of circle plot . . . . .	36
4.5	API collapse equation in neutral stress datum . . . . .	39
4.6	Superimposition of API collapse equation in the horizontal ellipse plot	42
4.7	Superimposition of API axial limits in the horizontal ellipse . . . . .	43
4.7.1	Slanted line in horizontal ellipse . . . . .	44
4.7.2	Color scheme approach in the horizontal ellipse . . . . .	49
4.8	New case . . . . .	50
<b>5</b>	<b>Conclusions</b>	<b>55</b>
<b>A</b>	<b>Equation limit line</b>	<b>60</b>
<b>B</b>	<b>Derivation of equation 4.8</b>	<b>68</b>

# List of Figures

2.1	Casing types and tubing in a well. . . . .	4
2.2	Principal stresses on a pipe (Bellarby by permission, 2009). . . . .	5
2.3	Yield strength (Bellarby by permission, 2009). . . . .	7
2.4	Collapse types for N80 pipe (Bellarby by permission, 2009). . . . .	10
2.5	True and effective forces in a pipe. . . . .	13
2.6	Circle of plasticity . . . . .	14
2.7	Ellipse of plasticity . . . . .	14
3.1	Ellipse of plasticity with API limits . . . . .	19
4.1	Comparison of theoretical model and former API collapse equation. . . . .	23
4.2	Design limits plot for 3 <sup>1</sup> / <sub>2</sub> in, 12.7 lb/ft, L80 pipe. Built with data from Goodman et al., 2017. . . . .	24
4.3	Loads with same axial stress and different pressure in the approach from Goodman et al. . . . .	25
4.4	Design limits plot from commercial software for loads with safe axial tension force. . . . .	27
4.5	Design limit plot from commercial software including a load with unsafe axial force. . . . .	28
4.6	Design limit plot from commercial software for loads with safe axial compression stress and burst. . . . .	29

4.7	Design limit plot from commercial software including a load with unsafe axial stress and burst. . . . .	29
4.8	Design limit plot from commercial software including a load with unsafe axial stress and collapse. . . . .	30
4.9	Design limit plot from commercial software including a load with unsafe axial stress and collapse. . . . .	30
4.10	Ellipse of plasticity and API uniaxial limits with separated plots approach. . . . .	32
4.11	Ellipse of plasticity using the slanted line approach for an unsafe load. . . . .	34
4.12	Ellipse of plasticity using the slanted line approach for a safe load. . . . .	35
4.13	Ellipse of plasticity and API limits using color scheme. . . . .	36
4.14	Comparison of slanted ellipse and circle of plasticity (expressed as an horizontal ellipse). . . . .	37
4.15	Neutral equilibrium in slanted and horizontal ellipses for a pipe with $\beta = 7.1673$ and $D/t = 13.2530$ . . . . .	39
4.16	Application of the approach from Goodman et al. to the horizontal ellipse. . . . .	43
4.17	Application of the same approach as the commercial software to the horizontal ellipse. . . . .	44
4.18	API limit superimposed in the horizontal ellipse using the slanted line approach. . . . .	47
4.19	Slanted line approach for a load with equal internal and external pressures. . . . .	48
4.20	Color scheme approach in the horizontal ellipse. . . . .	49
4.21	Color scheme applied to the horizontal ellipse when multiple loads are included. . . . .	50
4.22	Plot from commercial software for the new case. . . . .	52
4.23	Plot using Goodman et al. approach in slanted ellipse for the new case. . . . .	52

4.24	Plot using horizontal ellipse with the colors scheme for the new case.	52
A.1	Test data vs. API collapse limit for 7 in, 20 lb/ft, K55 pipe. . . . .	60
A.2	Test data vs. API collapse limit for 7 in, 23 lb/ft, K55 pipe. . . . .	61
A.3	Test data vs. API collapse limit for 7 in, 26 lb/ft, K55 pipe. . . . .	61
A.4	Test data vs. API collapse limit for 7 in, 23 lb/ft, N80 pipe. . . . .	62
A.5	Test data vs. API collapse limit for 7 in, 26 lb/ft, N80 pipe. . . . .	62
A.6	Test data vs. API collapse limit for 7 in, 32 lb/ft, N80 pipe. . . . .	63
A.7	Test data vs. API collapse limit for 7 in, 38 lb/ft, N80 pipe. . . . .	63
A.8	Test data vs. API collapse limit for 7 in, 23 lb/ft, P110 pipe. . . . .	64
A.9	Test data vs. API collapse limit for 7 in, 26 lb/ft, P110 pipe. . . . .	64
A.10	Test data vs. API collapse limit for 7 in, 32 lb/ft, P110 pipe. . . . .	65
A.11	Test data vs. API collapse limit for 7 in, 38 lb/ft, P110 pipe. . . . .	65
A.12	Collapse ellipse for 7 in, 23 lb/ft, K55 pipe. . . . .	66
A.13	Collapse ellipse for 7 in, 32 lb/ft, N80 pipe. . . . .	66
A.14	Collapse ellipse for 7 in, 26 lb/ft, P110 pipe. . . . .	67



# List of Tables

3.1	Well design information in example from Goodman et al., 2017. . . . .	20
3.2	Load cases for 3 <sup>1</sup> / <sub>2</sub> in, 12.7 lb/ft, L80 pipe (Goodman et al., 2017). . . . .	21
4.1	Loads for evaluation of the approach from Goodman et al. . . . . . .	25
4.2	Loads for evaluation of tension limit in commercial software. . . . . .	26
4.3	Loads for evaluation of compression limit in commercial software. . . . .	28
4.4	Well design for new load case example. . . . . . . . . . . . . . . . . . . .	51
4.5	Load cases for 5 <sup>1</sup> / <sub>2</sub> in, 23 lb/ft, N80 pipe example. . . . . . . . . . . . . .	51

# Abbreviations

**APB** Annular Pressure Buildup.

**API** American Petroleum Institute.

**HPHT** High Pressure, High Temperature.

**RKB** Rotary Kelly Bushing.

**TOC** Top Of Cement.

# Chapter 1

## Introduction

Casing and tubing are the structural support of a well and therefore, the successful production of subsurface fluids depends on a proper selection of them. They represent also a significant percentage of the costs of a drilling project. A correct selection implies, therefore, ensuring that the tubulars will withstand the loads in the well while being as economical as possible. As wells become more challenging due to higher depths, temperatures, and pressures that create higher loads, choosing the correct casing and tubing becomes critical to make projects viable.

In order to improve the selection process of casings and tubing, continuous research has been done to find equations that accurately predict the failure of pipes under individual and combined loads. From these failures, collapse is maybe the more complex because it is an instability problem. Recently, the American Petroleum Institute (API) has presented a new equation that involves triaxial loads and therefore offers a more accurate calculation of collapse pressure under combined loads. This new equation relates to the work made by Arthur Lubinski more than 40 years ago and implies a change in the horizontal axis of the design limits plot, creating incompatibility with the axial compression and tension limits. Some solutions have been presented, however, those are only approximations that in many cases can lead to misunderstandings of those limits. This project offers an approach to evaluate this incompatibility and propose new methods to plot the ellipse of plasticity with the uniaxial and triaxial equations from API.

The ellipse was developed from the circle of plasticity, which was never adopted by the industry even if it presents significant advantages. A common argument to prefer the ellipse is the API limits cannot be superimposed on the circle. The present work evaluates this argument against the circle and presents a new approach to make it

compatible with the latest API equation, reinforcing its convenience as a tool for well design. The advantages of the circle, like its symmetry and the convenience of its axes, are also discussed.

The study starts with a review of the theory behind the evaluation of loads, mechanical properties of casing and tubing, and a summarized history of the pressure collapse equations in the API 5C3 standard. Afterward, the current industry approaches to plotting the ellipse of plasticity together with the API limits are analyzed; new approaches with their respective equations are presented and evaluated to choose the most convenient one. A new methodology to implement the circle making it compatible with the latest API equations is introduced. The results are discussed, to finally present conclusions and recommendations for future studies in the subject. It is important to note before hand that all calculations in the project disregard buckling and instead assume that all negative axial forces will create only compression.

# Chapter 2

## Theory

The correct selection of casing and tubing is made based on the mechanical properties and equations presented in this chapter. Special emphasis is given to collapse as it is the main topic of these project, thus, the history of the equations used by the American Petroleum Institute (API) to calculate this pressure is also presented.

### 2.1 Casing and tubing

A casing is defined as a pipe lowered into an open hole in a well and cemented in place (Ramsey, n.d.). According to their size, location, and function, casings can be divided into six different types:

- **Conductor casing:** It is the first string to be installed in the well. Its main functions are to isolate unconsolidated formations and protect against shallow gas. The conductor casing can be drilled and cemented to surface (mudline in offshore wells) or hammered.
- **Surface casing:** Installed to provide support for the wellhead equipment, protect shallow aquifers, and prevent lost circulation. This casing is usually cemented to surface (mudline).
- **Intermediate casing:** Its main function is to isolate unstable hole sections and formations with hydrocarbons that are not of interest. This casing is usually set in the transition zone from normal to abnormal pressure. For long wells, multiple intermediate casing may be required. This casing is not usually cemented to surface.

- **Production casing:** Used to isolate secondary production zones and contain pressures in case of a tubing leak. This casing is usually set at the top of the main production zone or some meters above. It is not usually cemented to surface but due to its functions, verification of a good cement job is very important.
- **Liner:** It is a casing string that hangs from a previous one. Some reasons to avoid extending a casing to surface are costs, rig limitations, and hydraulic performance. The most common type is the production liner, however, for long wells, it can be used in the intermediate section as well. Liners are usually cemented over their entire length.
- **Tieback:** Is a string used to connect a liner to the surface, providing additional pressure protection. It can be used to protect a worn casing or to isolate intermediate strings from production loads.

A tubing is a string of pipe that connects the reservoir with the surface, providing a conduit for the production or injection of fluids. It protects intermediate casing strings or tiebacks from the formation fluids and must be designed according to the well geometry, expected production rate, and reservoir fluids characteristics. Figure 2.1 present a typical well configuration, showing the different casing types and the tubing previously described.

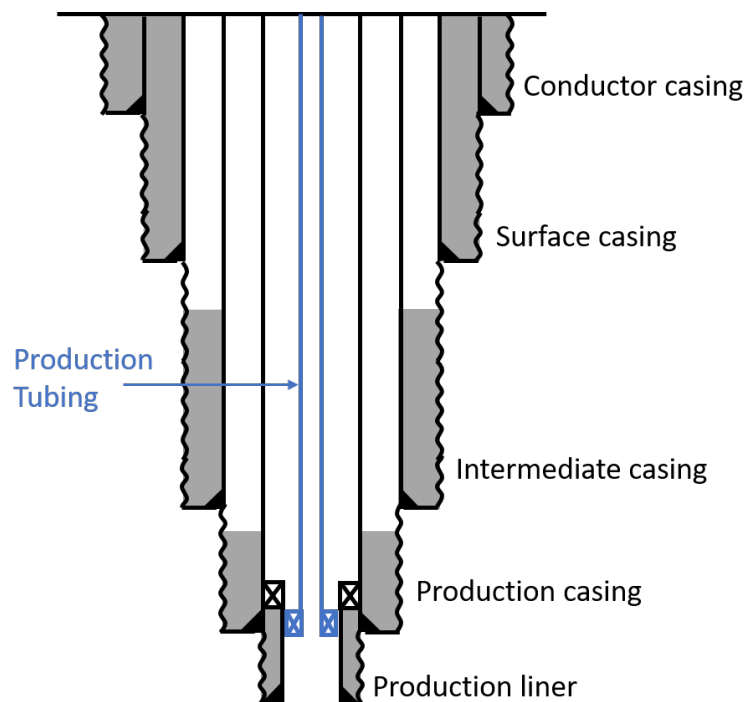


Figure 2.1: Casing types and tubing in a well.

## 2.2 Stress analysis in casing and tubing

When installed in a well, the casing and tubing strings will be subjected to different loads. The effects of these loads in the pipe can be mathematically expressed through the three principal stresses: axial stress ( $\sigma_a$ ), radial stress ( $\sigma_r$ ), and tangential or hoop stress ( $\sigma_t$  or  $\sigma_h$ ). These principal stresses are shown in figure 2.2. The capacity of the pipe to handle those loads is given by its mechanical properties.

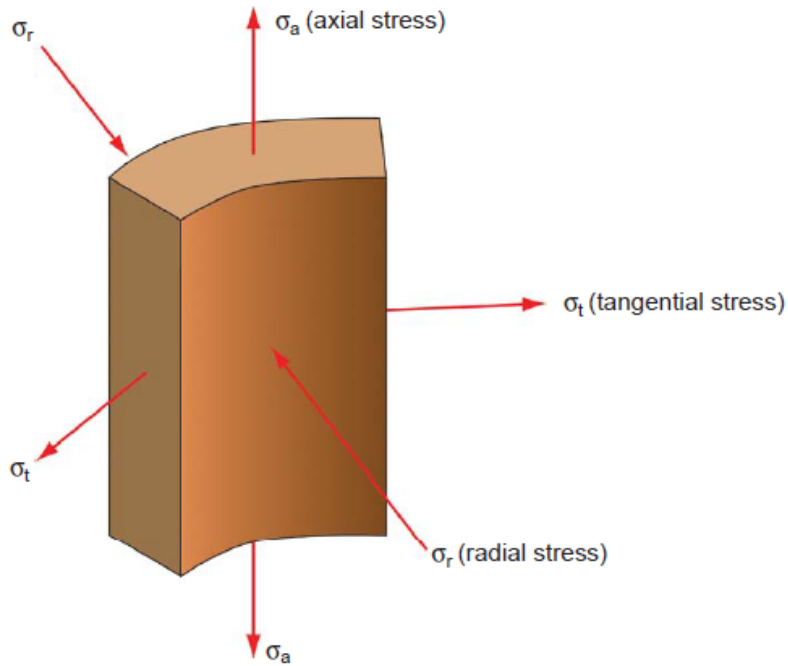


Figure 2.2: Principal stresses on a pipe (Bellarby by permission, 2009).

The axial stress is created by tension or compression forces, for example, the weight of the pipe will create tension on the top of the string; it can also be created by the internal pressure when one of the pipe endings is closed. The tangential or hoop stress is created by internal pressures which exert circumferential forces on the pipe (like trying to separate it in two halves). The radial stress is created by the difference in pressure and area in the inside and outside of the pipe. When the wall of the pipe is thick, the internal area will be notably smaller than the external area and therefore the force exerted in the inside will be higher than the force on the outside, creating radial stress.

## 2.2.1 Cylinders types and stress calculations

The dependence of some of the principal stresses on the inside and outside areas of the pipe has lead to divide the study of cylindrical structures into two categories according to the relation between the inside diameter ( $d$ ) and the thickness ( $t$ ) (Belayneh, 2019):

- Thin walled cylinders if:

$$\frac{d}{t} > 20$$

In this case, the pipe is assumed as a surface due to the small thickness of its wall and therefore, no radial stress exist. The two other principal stresses are given as:

$$\sigma_h = \frac{p_i r_i}{t} \quad (2.1)$$

$$\sigma_a = \frac{p_i r_i}{2t} \quad (2.2)$$

The axial stress exists only when there is a closed-ended pipe. If the ends are open, no axial stress is present.

- Thick walled cylinders if:

$$\frac{d}{t} < 20$$

In this case, the difference in internal and external areas will influence the application of forces in the pipe. The three principal stresses are given by equations 2.3, 2.4 and 2.5, from which the first two formulations correspond to the Lamé equations:

$$\sigma_r = \frac{p_i r_i^2 - p_o r_o^2}{r_o^2 - r_i^2} + \frac{r_i^2 r_o^2 (p_o - p_i)}{(r_o^2 - r_i^2) r^2} \quad (2.3)$$

$$\sigma_h = \frac{p_i r_i^2 - p_o r_o^2}{r_o^2 - r_i^2} - \frac{r_i^2 r_o^2 (p_o - p_i)}{(r_o^2 - r_i^2) r^2} \quad (2.4)$$

$$\sigma_a = \frac{p_i r_i^2 - p_o r_o^2}{r_o^2 - r_i^2} + \frac{F_a}{A_s} \quad (2.5)$$

The ability of a pipe to withstand these stresses depends on the mechanical properties described in the following subsections.



## 2.2.2 Yield strength

When an axial force in the form of tension is applied to a pipe, the material is subjected to stress and will deform according to Hooke's law. When the stress is plotted as a function of the deformation as in figure 2.3, two regions are observed: a linear region (from origin to point P) where the pipe deforms in a reversible or elastic way and a nonlinear region (to the right of the point P) in which the deformation is irreversible or plastic. The point at which the deformation changes from elastic to plastic is called the yield point and the plastic deformation is known as yielding.

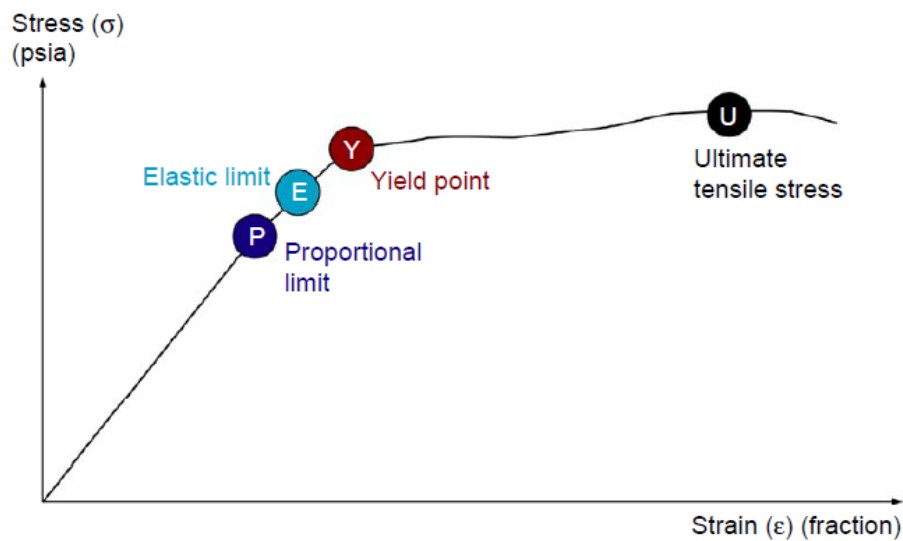


Figure 2.3: Yield strength (Bellarby by permission, 2009).

API defines the yield strength as “the axial load required to yield the pipe in the absence of internal or external pressure, bending and torsion” (API, 2018). The API grade defines the minimum strength of the pipe, for example, an N80 pipe will have a yield strength of 80000 psi. With this information the maximum axial force that can be applied to the pipe can be determined by equation 2.6.

$$F_a = \frac{Y}{A_s} \quad (2.6)$$

In the case of compression, the yield strength is assumed to be the same as in tension, nevertheless, as buckling can occur, the pipe can fail before reaching the yield strength. This is however not considered in equation 2.6 (Mitchell et al., 2011).

### 2.2.3 Burst pressure

The burst pressure is the minimum internal pressure that will cause an irreversible deformation in the pipe in the absence of axial loads or external pressure. The API, 2018 standard uses the Barlow equation for the calculation of the internal yield pressure of tubulars. This is not a formula for pipe rupture, but only for internal pressure and therefore is a conservative approach (Byrom, 2007). The formula is:

$$p_{burst} = 0.875 \frac{2Yt}{D} \quad (2.7)$$

Where the 0.875 factor corresponds to a 12.5% allowance for wall thickness variation as will be discussed in the critical dimensions section. The Barlow equation is the result of a one-dimensional analysis assuming only hoop stress in a thin-walled cylinder. Recent studies have, however, validated the equation by showing the same result for a thick-walled cylinder (Adams et al., 2018).

### 2.2.4 Collapse pressure

The collapse pressure is the minimum external pressure that will cause an irreversible deformation in the pipe. It is probably the most common type of failure after corrosion and wear (Byrom, 2007). Collapse is an instability problem that requires the eventual yield of the entire pipe body around the pipe and therefore is a more complex study than burst (Bellarby, 2009). This means that for high values of  $D/t$  ratio, the pipe will fail by buckling of the wall at stresses that may be considerably below the yield point (Windenburg & Trilling, 1934). As a consequence of this complexity API has defined four types of collapse:

- **Yield collapse:** It is the external pressure that will cause minimum yield stress on the inside wall of the pipe, therefore, it is not a real collapse pressure. This is a consequence of the fact that for pipes with  $D/t < 15$ , the tangential stress exceeds the yield strength of the material before any instability failure occurs (Mitchell et al., 2006). The yield collapse is calculated with equation 2.8.

$$p_y = 2Y \left[ \frac{D/t - 1}{(D/t)^2} \right] \quad (2.8)$$

- **Plastic collapse:** The pressure for this type of collapse is calculated using the formula presented in equation 2.9, which was obtained by applying a regression to the data obtained from 2488 test. This collapse type occurs when the stress required to buckle the wall of the pipe needs to be higher than the yield stress of the material (Pattillo, 1985b).

$$p_p = Y \left[ \frac{A}{D/t} - B \right] - C \quad (2.9)$$

- **Transition collapse:** Due to a gap between the plastic and elastic regimes it was necessary to include a numerical fit as the transition between them, which is expressed by equation 2.10.

$$p_t = Y \left( \frac{F}{D/t} - G \right) \quad (2.10)$$

- **Elastic collapse:** This collapse regime is independent of the yield strength, because the hoop stress leading to buckling is below the yield stress of the material (Pattillo, 1985b). It is calculated by equation 2.11.

$$p_e = \frac{46.95 \times 10^6}{(D/t)(D/t - 1)^2} \quad (2.11)$$

Most of the pipes used in the oil industry collapse in the “plastic” or “transition” regimes (Mitchell et al., 2006). The selection of the pressure equation is based on the outside diameter to thickness ratio  $D/t$  and the grade of the pipe according to API tables and formulas. An example of the application of these formulas is shown in figure 2.4.

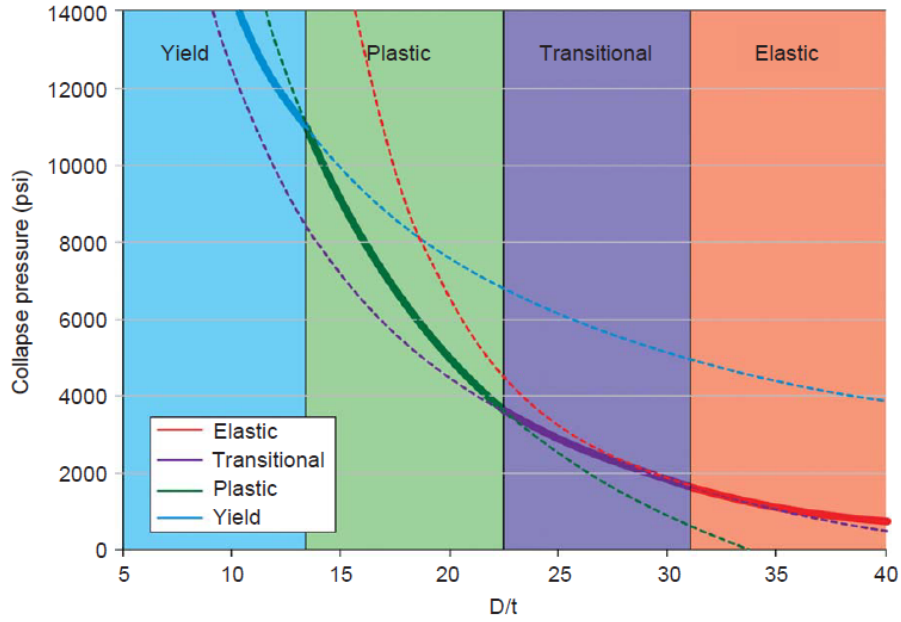


Figure 2.4: Collapse types for N80 pipe (Bellarby by permission, 2009).

The values of factors  $A$ ,  $B$ ,  $C$ ,  $D$ ,  $F$  in equations 2.9 and 2.10 are also given by the API standard in tables and as formulas, and the pressure values calculated with those constants are given in API 5C2.

Equations 2.8 to 2.11 are valid for uniaxial loads. To account for internal pressure and axial stress, the yield strength on those equations  $Y$  must be corrected to  $Y_*$ . The 2018 version of the API 5C3 standard indicates that this can be done with equation 2.12.

$$Y_* = \left[ \sqrt{1 - 0.75 \left( \frac{\sigma_a + p_i}{Y} \right)^2} - 0.5 \left( \frac{\sigma_a + p_i}{Y} \right) \right] Y \quad (2.12)$$

When a pipe wall begins to buckle, under collapse, the buckle will propagate along the tube at a much lower pressure than the one that caused the initial collapse. For this reason, the presence of defects in the casing, like ovality or reduced wall thickness, can significantly reduce its resistance to collapse. These defects are taken into account in the design process by the use of design factors when calculating combined loads. Some authors have developed new formulas for collapse calculations including defects (see Klever & Tamano, 2004), however, those are not yet included in the API standard and therefore are not studied in this project.

### 2.2.5 Triaxial loads

In a real well environment, pipes are not subjected to only one kind of load, but instead to a combination of two or the three of them. The effect of the combined loads is called the equivalent stress and can be determined using the Von Mises criterion which is based on the maximum distortion energy theory. In the absence of bending and torsion, which is the situation of interest in this work, API, 2018 indicates that the criterion can be expressed by equation 2.13.

$$\sigma_{VME} = \sqrt{\sigma_r^2 + \sigma_h^2 + \sigma_a^2 + \sigma_r\sigma_h - \sigma_r\sigma_a - \sigma_h\sigma_a} \quad (2.13)$$

When the equivalent stress is lower than the yield strength ( $\sigma_{VME} < Y$ ), the tubular is in the elastic stress regime and therefore will not suffer permanent deformation. For pipes without bending or torsion, the Von Mises stress will be the highest at the inner wall and the pipe will start yielding at this point. The use of this criterion explains the existence of equation 2.12 to calculate the collapse pressure in situations where more than one load is acting on the pipe at the same time.

### 2.2.6 Critical dimensions

As a result of the manufacturing process, pipes can present defects, that will reduce their ability to withstand loads. When the dimensions are not exact, for example, the region in which the thickness is the lowest will see the highest stress when a force is applied. To account for this, the critical dimensions are included when calculating the mechanical properties of the pipe. The clearest example is the 0.875 factor present in the Barlow formula to calculate the burst pressure, which implies a manufacturing tolerance of 12.5% in the wall thickness. While this burst factor is the only one explicitly recommended by API, commercial software allow the use of critical dimensions for all mechanical properties and even for the triaxial load. In the latest case, the critical dimensions can be expressed in terms of the hoop stress or for the total triaxial load calculation. The default value in the most commonly used software is 0.875 (87.5%) for hoop stress. As this project follows the API standards, only the 0.875 factor for burst calculation will be used, while assuming 100% of critical dimensions for the other properties.

## 2.3 Effective force

When studying buckling in pipes, Lubinski, 1975, observed that when exposed to internal and external pressure, the behavior of a tubular was not as expected and explained this difference to be caused by a “fictitious force”, which he later was expressed in terms of stress as equation 2.14.

$$\Delta\sigma_a = \sigma_a - \sigma_n \quad (2.14)$$

Where  $\sigma_n$  is the neutral axial stress, denoted as:

$$\sigma_n = \frac{d^2 p_i - D^2 p_o}{D^2 - d^2} \quad (2.15)$$

Sparks, 1984, lately, offered a simpler mathematical definition of this effective force using equation 2.16.

$$F_e = F_R + A_o p_o - A_i p_i \quad (2.16)$$

The effective force is a consequence of disregarding the axial forces created by the internal and external pressures (tension and compression respectively) which, however, are not able to create or prevent buckling. This means that, when a pipe is submerged in fluids in a well, the hydraulic effects of those fluids need to be disregarded when evaluating the axial loads. The tubular will then behave as if there were no fluid and if the weight of the steel was simply decreased by the weight of the displaced fluid. When constant pressure is applied by a fluid inside a pipe, for example, the real force will increase, giving the impression that the pipe is totally in tension, however, the effective force can still indicate potential of buckling as observed in the fourth case in figure 2.5, in which  $T_R$  indicates real force (tension) and  $T_e$  indicates effective force (tension). When the pressure is applied on the outside of the pipe as in the right most case in the figure, the real force can indicate that the pipe will buckle while it is safe as showed by the effective force. Some other behaviors described by the effective force are presented in this figure.

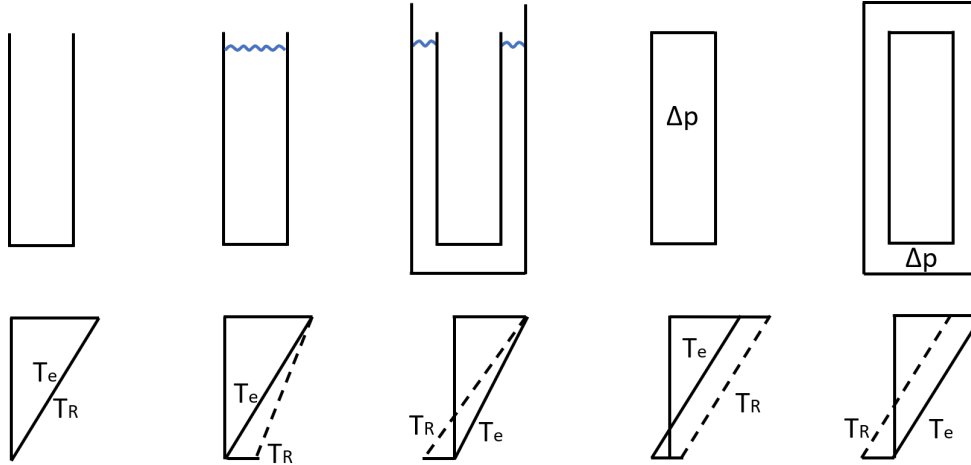


Figure 2.5: True and effective forces in a pipe.

The effective force is important in collapse because, as mentioned previously, it is an instability problem that implies the buckling of the pipe walls and therefore the hydraulic effects should be disregarded. The real force is however important for other types of calculations, for example when pipe stress and limits are considered.

## 2.4 Yield circle and ellipse

By inserting the Lamé equations in the Von Mises criterion equation and taking into consideration the concept of effective force, Lubinski, 1975, was able to develop an expression for the triaxial stress in a pipe. Equation 2.17 present the resulting relation which corresponds to a circle, therefore, he called it the “circle of plasticity” (see Figure 2.6).

$$[\Delta\sigma_a]^2 + \left[ \sqrt{3} \frac{D^2}{D^2 - d^2} (p_i - p_o) \right]^2 = Y^2 \quad (2.17)$$

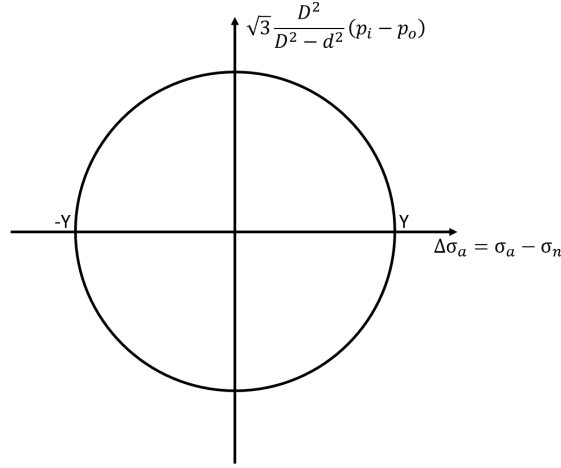


Figure 2.6: Circle of plasticity

By defining  $\Delta p = p_i - p_o$  and doing algebraic work, Lubinski adapted the circle equation to an ellipse formulation that can be expressed as equation 2.18.

$$\frac{p_o - p_i}{Y} \beta = \sqrt{1 - \frac{3}{4} \left( \frac{\sigma_a + p_i}{Y} \right)^2} \pm \frac{1}{2} \left( \frac{\sigma_a + p_i}{Y} \right) \quad (2.18)$$

Where  $\beta$  is a geometrical factor lately defined by Aasen and Aadnøy, 2003, and corresponding to:

$$\beta = \frac{(D/t)^2}{2(D/t - 1)} \quad (2.19)$$

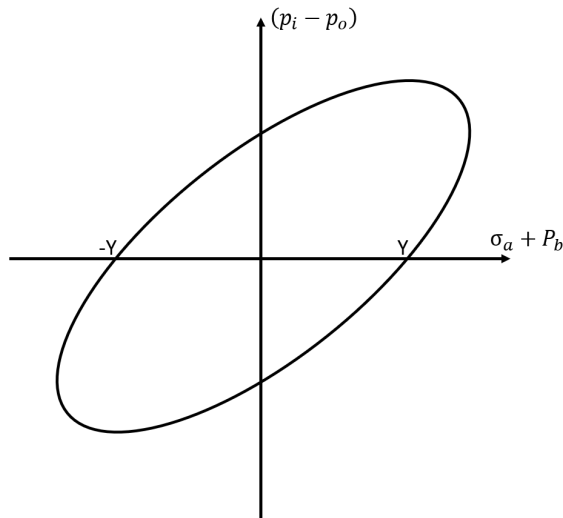


Figure 2.7: Ellipse of plasticity



Although the circle matched the experimental test results better, the ellipse has been the one in use until today. Recently some updates have been applied to it as presented later in the chapter.

## 2.5 History of API collapse equation

The collapse pressure equation used by the American Petroleum Institute (API) for their technical reports has changed over time. According to Goodman et al., 2017, the first attempt to developed a collapse equation was made in 1939, when the theoretical work by several authors led to a set of formulas, dividing collapse into yield, plastic and elastic. There was still a discontinuity between elastic and plastic limits that was filled with a transition collapse limit. These first equations assumed zero axial force and zero internal pressure.

Lately, some corrections were proposed to account for the influence of axial stress by converting the resulting collapse pressure into a reduced collapse pressure. This corrections had the form of the equation derived by Holmquist and Nadai, 1939 for the biaxial ellipse of plasticity. The industry got used to work with this biaxial ellipse equation and when in 1975 Lubinski developed his triaxial circle of plasticity, he adapted it to a triaxial ellipse.

In 1980, Clinedinst, 1980 proposed the most recent version of the collapse formulation to the API. However, the organization published a correction for only axial load that also took the form of the Holmquist and Nadai ellipse, but to find an "equivalent yield strenght". A new formulation was provided by API, 1989, to include both internal and external pressure. This new equation was presented as the "Effect of Internal Pressure Collapse":

$$p_E = p_c - \left(1 - \frac{2}{D/t}\right) p_i \quad (2.20)$$

In the 2008 version of API 5C3 (API, 2015), the equation was modified and a result described many years before by Pattillo, 1985a, was used to determine an effective collapse resistance due to the effect of internal pressure:

$$p_{ci} = p_c + \left(1 - \frac{2}{D/t}\right) p_i \quad (2.21)$$

Under this formulations, the API limits were easily superimposed on the biaxial

ellipse of plasticity. Based on suggestions made by Clinedinst, 1980, in 2015 an addendum was published by API with a new equation that represents “the combined loading equivalent grade, the equivalent yield strength in the presence of axial stress and internal pressure” (API, 2015). In 2018 the new equation was presented as official in the new version of the standard. In a recent paper, Goodman et al., 2017, questioned the reference of API for this new equation to Clindelinist, stating that the source was Lubinski, 1975. However, documents that Clindelinist send to the organization, show that he was aware of the work made by Lubinski and used it as a base to obtain his results, adapting it to the API formulations. In the same publication, Goodman et al. updated the triaxial ellipse equation to generalize it from just collapse with external pressure to a more general case of back up pressure ( $p_b$ ), which corresponds to internal pressure for burst and external pressure for collapse. The results are two independent equations for the burst and collapse halves of the plot. Equation 2.22 shows the result for the collapse half of the ellipse in terms of the geometrical factor  $\beta$ . It is the same as the API equation for yield collapse (equation 2.8) when  $Y_*$  (equation 2.12) is included.

$$p_i - p_b = \frac{Y}{\beta} \left[ \sqrt{1 - \frac{3}{4} \left( \frac{\sigma_a + p_i}{Y} \right)^2} - \frac{1}{2} \left( \frac{\sigma_a + p_i}{Y} \right) \right] \quad (2.22)$$

For the burst half of the ellipse, the result in term of the geometrical factor  $\beta$  is equation 2.23:

$$p_i - p_b = \frac{Y}{\beta} \left[ \sqrt{\frac{1}{j} - \frac{3}{4j^2} \left( \frac{\sigma_a + p_o}{Y} \right)^2} - \left( \frac{1}{2} \right) \left( \frac{k}{j} \right) \left( \frac{\sigma_a + p_o}{Y} \right) \right] \quad (2.23)$$

Where:

$$k = \frac{r_i^2}{r_o^2} \quad (2.24a)$$

$$j = \frac{3 + k^2}{4} \quad (2.24b)$$

When comparing equations 2.22 and 2.23, it can be noticed that for the same ellipse, the abscissa will take two different values:  $\sigma_a + p_o$  for the burst half of the plot and

$\sigma_a + p_i$  for the collapse half. This would be reflected in the plot by different slopes in both halves of the ellipse and a slight kink in the abscissa when  $p_i - p_b = 0$ .

With these latest developments, the API limits require now to be plotted against the triaxial ellipse of plasticity, instead of the biaxial ellipse. This new plot creates some incompatibilities with the uniaxial limits that are presented and discussed in the next chapter.

# Chapter 3

## Method

It was previously mentioned that the new collapse formulation in the API standards recalls the work made by Lubinski 40 years ago but focusing on the ellipse and not the circle of plasticity. One of the common arguments to avoid the use of the last one is that the API limits can not be shown in the same plot (Goodman et al., 2017). The methodology to be used to evaluate this affirmation is described in the present chapter, starting with a comparison between the previous and new API collapse formulations. Next, the ellipse plot is evaluated in terms of the 2018 equation. The ellipse of plasticity was, however, developed from the circle. This means that both are based on the same underlying theory and that the proposed approaches could be also applicable to the circle. To evaluate this, a new approach to making the circle more practical is presented and the mathematical development is done to make it compatible with the API limits.

### 3.1 Comparison of previous and new API equation

The equation to account for axial force and internal pressure in collapse calculations introduced in the 2008 version of API 5C3, represent an attempt to account for the effect of internal pressure. It is however just an approximation. To evaluate its accuracy, a formulation developed by Aasen and Aadnøy, 2003 and presented in equation 3.1 will be divided by the API equation. The resulting ratio will be plotted to present a graphical evaluation.

$$p_c = \frac{p_i(2\beta - 1) - \sigma_a + \sqrt{4Y^2 - 3(p_i + \sigma_a)^2}}{2\beta} \quad (3.1)$$

## 3.2 API equations and design limits plots

Figure 3.1 shows how the ellipse of plasticity is usually presented including the latest developments made by Goodman et al., 2017.

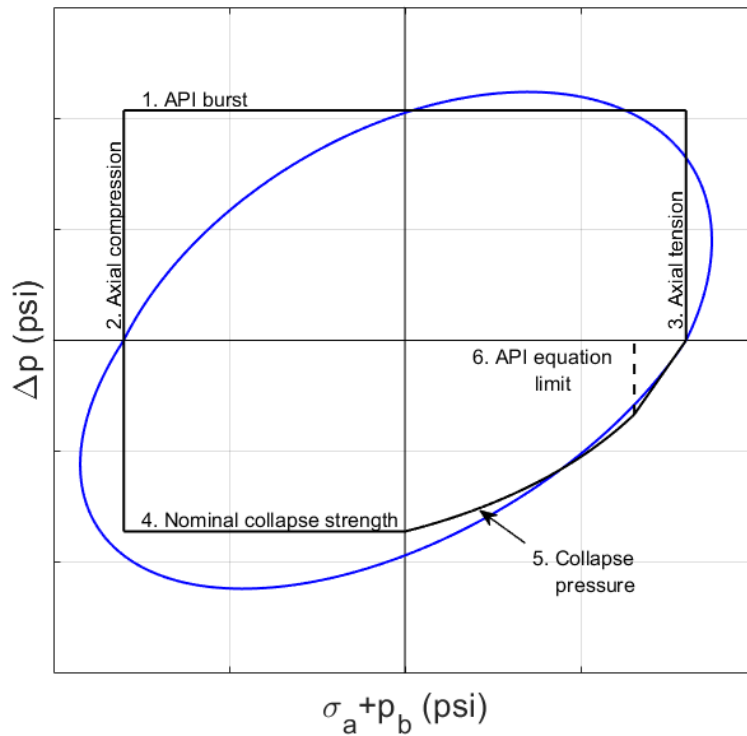


Figure 3.1: Ellipse of plasticity with API limits

In this figure, six different API limits are observed: (1) burst, (2) axial compression, (3) axial tension, (4) nominal collapse pressure, (5) deration of collapse for tension and internal pressure, and (6) the equation limit line. The limits 1 to 4 have been established by API through equations that are only applicable to uniaxial loads. The collapse pressure (5) is defined by API as a triaxial limit because it considers a collapse load under the presence of axial stress and external pressure. The equation limit line (6) is a consequence of the limitations of the collapse equations (which are valid only for  $Y_* \leq 24000 \text{ psi}$ ) and can, therefore, be considered as a triaxial limit as well. It is presented as a vertical line (dashed line in the figure) in journal

publications (see Goodman et al., 2017) while the literature (see Bellarby, 2009) and commercial software use a straight line that connects the limit with the value of the yield strength on the abscissa. The API standard does not present a justification for this limitation of the equation, therefore, using some test results and documents sent to the API by Clinedinst (Clinedinst, 1981), a study was performed to select the best way to plot it, resulting in the use of a straight line that connects the collapse curve with the value of the yield strength on the abscissa as done in the commercial software and literature. This analysis is presented in appendix A.

Uniaxial and triaxial limits are not compatible. When constructing the plot using the most recent API equations, the horizontal lines (1 and 4) are independent of loads and therefore fixed for all cases. The vertical lines (2 and 3), however, become dependent on the load case and will require to be moved in the horizontal axis as discussed in the next chapter.

The two solutions used by the industry to solve this incompatibility will be evaluated independently by plotting individual loads and discussing their strengths and weaknesses. Three new methods will be also proposed and evaluated to choose the one that offers the best solution. All approaches will be compared using the example case from Goodman et al., 2017, which will be recreated from the data in table 3.1. It corresponds to a 17500 ft offshore vertical well with a water depth of 300 ft, an air gap of 100 ft, and a surface wellhead 40 ft below the rotary table (RKB). The temperature profile is 40°F at surface and mudline (400 ft from RKB) and 380°F at 17500 ft. The tubing packer is set at 17000 ft. The main focus will be on the 3<sup>1</sup>/<sub>2</sub> in, 12.7 lb/ft, L80 pipe which information is showed in table 3.2. This pipe is chosen because it falls in the yield collapse regime and therefore its collapse limit curve will overlap the one of the ellipse of plasticity, simplifying the analysis.

Pipe	Measured depth (ft)			Hole size (in)	Pick up force (lbs)
	Hanger	TOC	Shoe		
20 in, 94 lb/ft, K55	40	450	2000	26	400000
13 <sup>3</sup> / <sub>8</sub> in, 72 lb/ft, N80	40	6100	9700	17 <sup>1</sup> / <sub>2</sub>	
9 <sup>5</sup> / <sub>8</sub> in, 53.5 lb/ft, N80	40	9500	15000	12 <sup>1</sup> / <sub>4</sub>	
7 in, 38 lb/ft, T95 Tie-back	14800	14800	17500	8 <sup>1</sup> / <sub>2</sub>	300000
7 in, 38 lb/ft, T95 Liner	40	14800	14800		
3 <sup>1</sup> / <sub>2</sub> in, 12.7 lb/ft, L80	40		17000		

Table 3.1: Well design information in example from Goodman et al., 2017.

Load	Load description		
	$p_i$ (psi)	$p_o$ (psi)	Temperature
Acid job (burst)	7218 psi @ 40 ft and 14700 psi @ 17000 ft	10 ppg brine to 17000 ft	50°F from 40 to 400 ft and 111°F @17000 ft
ABP (collapse)	10 ppg brine to 17000 ft	2500 psi on top of 10 ppg brine	50°F from 40 to 400 ft and 111°F @17000 ft

Table 3.2: Load cases for 3<sup>1</sup>/<sub>2</sub> in, 12.7 lb/ft, L80 pipe (Goodman et al., 2017).

The detail of the loads used, the resulting plots, and the corresponding discussions are presented in the following chapter.

### 3.3 Implementation of the circle of plasticity

To call attention to the circle of plasticity, the first step is finding the most convenient axes that make it more practical for engineering purposes. This is done by algebraic manipulation of the original formulation presented in equation 2.17. The resulting plot will be compared and evaluated against the currently used ellipse to discuss its advantages.

### 3.4 API collapse equation in neutral stress datum

Once the axes for the plot of the circle have been defined, it is necessary to find a way to adapt the API triaxial collapse limit to it. This will be achieved by using equations 2.14 and 2.15 to demonstrate the relation between the zero axial stress datum and the neutral axial stress datum and then reformulate this relation in terms of the new API collapse equation. The axial limits will be adjusted by applying the approaches proposed for the ellipse in the new circle plot.

# Chapter 4

## Results and discussion

The mathematical derivations and plots resulting from the application of the methodology described in the previous chapter are introduced now. Some numerical examples are included as part of the discussion and a new load case that summarizes the outcomes of the project is presented.

### 4.1 Discussion of new API equation

The theoretical model by Aasen and Aadnøy presented in chapter 3 can be adjusted for zero axial force, to obtain equation 4.1. This new formulation can be used to quantify the inaccuracy of the 2008 API collapse equation.

$$p_c = \frac{p_i(2\beta - 1) + \sqrt{4Y^2 - 3p_i^2}}{2\beta} \quad (4.1)$$

For a yield collapse regime, using the geometrical factor from equation 2.19, equation 2.21 can be expressed as:

$$p_{ci} = \frac{Y}{\beta} + \left(1 - \frac{2}{D/t}\right) p_i \quad (4.2)$$

Now equations 4.1 and 4.2 can be compared by dividing the first by the second one:

$$\frac{p_c}{p_{ci}} = \frac{p_{true}}{p_{approx}} = \frac{\frac{p_i(2\beta-1) + \sqrt{4Y^2 - 3p_i^2}}{2\beta}}{\frac{Y}{\beta} + \left(1 - \frac{2}{D/t}\right) p_i}$$



Multiplying nominator and denominator by  $2\beta$ :

$$\frac{p_c}{p_{ci}} = \frac{p_{true}}{p_{approx}} = \frac{p_i (2\beta - 1) + \sqrt{4Y^2 - 3p_i^2}}{2Y + 2\beta \left(1 - \frac{2}{D/t}\right) p_i}$$

The result of plotting this relation as a function of the  $D/t$  ratio for different values of internal pressure is presented in figure 4.1.

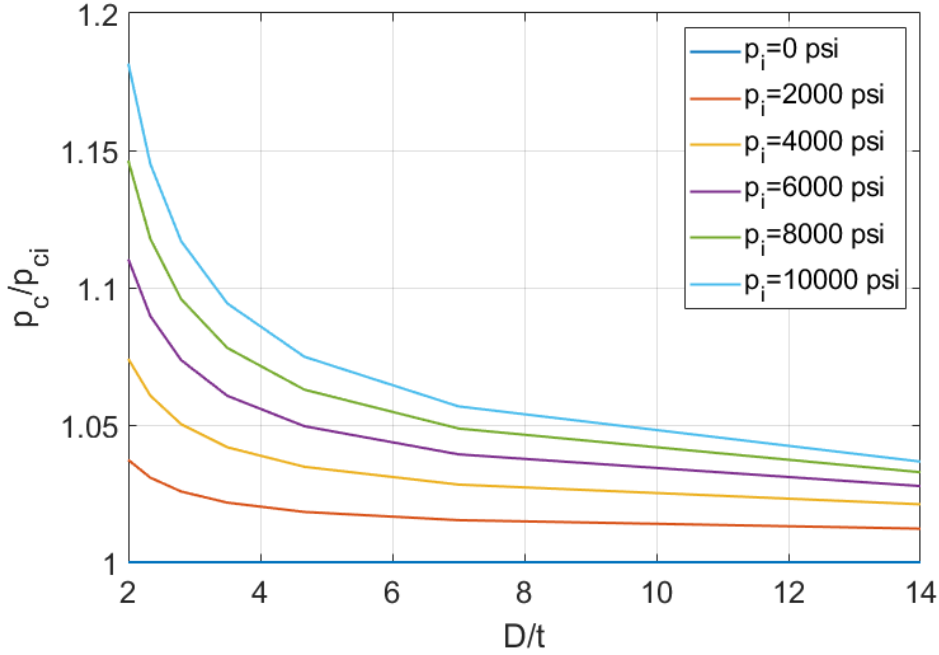


Figure 4.1: Comparison of theoretical model and former API collapse equation.

In this figure, a  $p_c/p_{ci}$  equal to one indicates that the 2008 API equation gives the same results as the theoretical model. This is the case only when  $p_i = 0 \text{ psi}$ , which represents a uniaxial load. As the ratio moves away from one, the API equation becomes more conservative. Low values of  $D/t$  that are a consequence of a thicker pipe wall, corresponds to higher  $p_c/p_{ci}$  and therefore the API equation is more inaccurate. The same happens as internal pressure increases. The previous model of API collapse equation is conservative but it can still be acceptable for thin-walled pipes under low pressures regimes. However, for thick-walled tubulars under higher pressure loads, the equation can involve a notable error, leading to too conservative designs that will result in higher costs.

The 2018 equation is based on the same underlying theory as the model by Aasen and Aadnøy, 2003 and therefore the results will be identical. This highlights the importance of this new formulation, as it will allow reducing the casing and tubing

cost due to its better accuracy that is reflected in more optimistic predictions of collapse pressures. The only challenge with this new equation is that when plotting it, the horizontal axis will become  $\sigma_a + p_b$ , creating complications when the uniaxial limits need to be superimposed. The following sections present a more detailed discussion about this.

## 4.2 Evaluation of current industry approaches to plot API limits

The industry has made some attempts to solve the incompatibility between the new API collapse equation and the uniaxial limits by doing some modifications to the plot presented in figure 3.1. One solution was presented by Goodman et al., 2017 and another one by industry-standard commercial software.

### 4.2.1 Goodman et al.

The approach presented by Goodman et al., 2017 uses  $\Delta p = p_i - p_o$  in the ordinate and  $\sigma_a + p_b$  in the abscissa of the design limits plot.  $p_b$  is the backup pressure that corresponds to the external pressure for the burst half of the ellipse and the internal pressure for the collapse half. The resulting plot is shown in figure 4.2. As indicated previously, the focus is set on the 3<sup>1</sup>/<sub>2</sub> in, 12.7 lb/ft, L80 pipe.

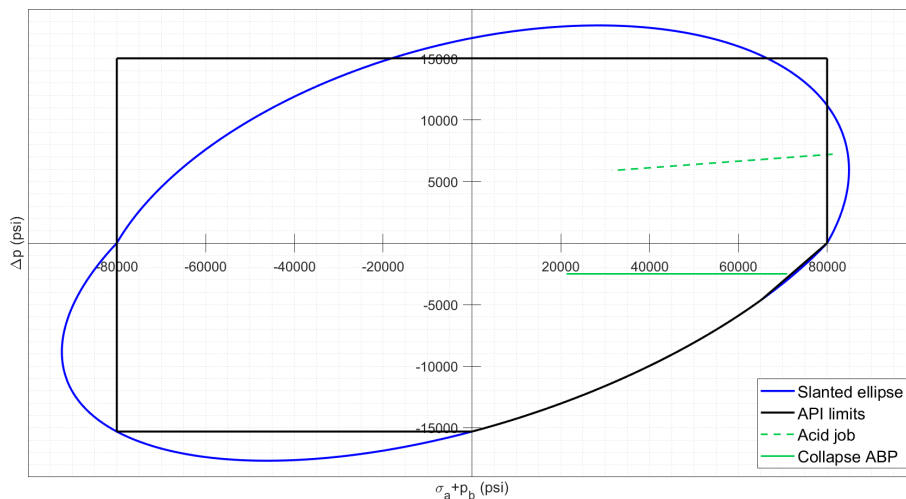


Figure 4.2: Design limits plot for 3<sup>1</sup>/<sub>2</sub> in, 12.7 lb/ft, L80 pipe. Built with data from Goodman et al., 2017.

This plot uses stress units in the abscissa, which allows to have the same units in both axes and is consistent with API. The API uniaxial limits are plotted as fixed straight lines: for the axial limits, vertical lines are used at the positive and negative values of yield strength ( $\sigma_a + p_b = \pm Y$ ). The burst and collapse limits are shown as horizontal lines at  $\Delta p = p_{burst}$  and  $\Delta p = p_{collapse}$  respectively. A vertical line marks the “ $Y_* \leq 24000 \text{ psi}$ ” limit. This is a practical approach to present all information in one plot and, for the loads presented in their paper, gives the impression of being accurate. However, it is not correct and can lead to confusion, as happens in figure 4.3. This plots uses the same pipe, therefore the ellipse and limits are the same, but the loads are the cases 1 and 2 from table 4.1.

Cases	$\sigma_a$ (psi)	$p_i$ (psi)	$p_o$ (psi)	$\sigma_a + p_o$ (psi)
Load 1	79000	7218	0	79000
Load 2	79000	7218	2000	81000

Table 4.1: Loads for evaluation of the approach from Goodman et al.

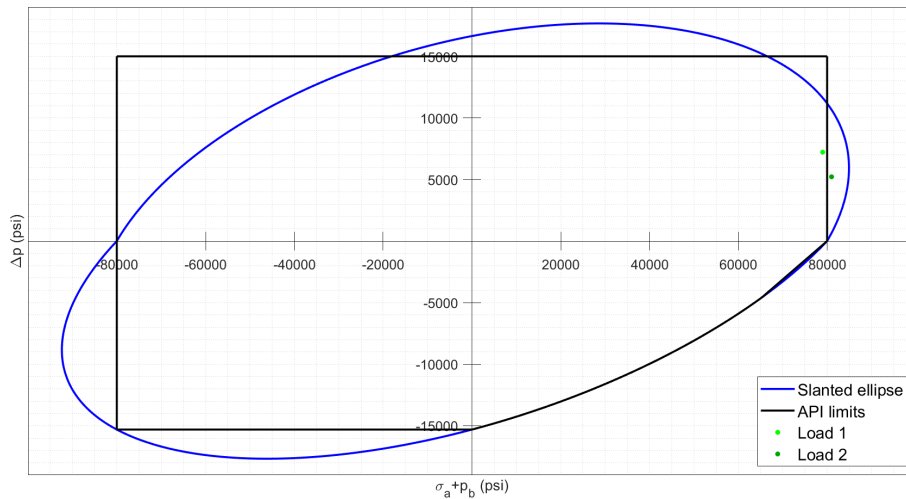


Figure 4.3: Loads with same axial stress and different pressure in the approach from Goodman et al.

Both loads in figure 4.3 have the same axial force, which is lower than the yield strength, but they appear on different sides of the tension limit, making load 2 look unsafe. This happens due to the presence of an external pressure of 2000 psi for this second case. To make sure that both loads are inside the limit, it should be displaced at least 2000 psi to the right. The fixed-line for tension is only true when  $p_o = 0 \text{ psi}$ . In a more strict perspective, it is only valid when  $p_i = p_o = 0 \text{ psi}$ , corresponding to the point  $(Y,0)$ , as this is a real uniaxial load that can be compared with a uniaxial limit. For loads with  $p_o > 0$ , this approach is not valid. In the same way, the

compression limit is only true for  $p_o = 0 \text{ psi}$  as the values in the negative side of the abscissa for  $\sigma_a < -Y$  will never be above the negative of the yield strength. As a general case, for cases where  $p_o \neq 0 \text{ psi}$ , there will be a family of lines that represent the axial limits according to the value of the external pressure.

## 4.2.2 Commercial software approach

The most used commercial software for well design presents the ellipse plot using force as the units for the abscissa which they call “Equivalent axial load”. This is practical in terms of engineering calculations as stress is never measured in operations, but makes it less intuitive when reading the API limits values. The equation limit is defined by a straight line that joins the last point in the collapse curve (the pressure corresponding to  $Y_* = 24000 \text{ psi}$ ) with the coordinate  $(Y,0)$ . To solve the problem of needing multiple lines for the axial limits in the plot, the software uses an algorithm that moves the lines to make sure that all unsafe loads are outside the limits. To verify the accuracy of this algorithm, the five loads in table 4.2 were evaluated for a  $3\frac{1}{2}$  in, 12.7 lb/ft, L80 pipe, the resulting plot for the cases 1 to 4 is shown in figure 4.4.

Cases	$\sigma_a$ (psi)	$p_i$ (psi)	$p_o$ (psi)	$\sigma_a + p_o$ (psi)
Load 1	79000	7218	0	79000
Load 2	79000	7218	2000	81000
Load 3	79000	7218	6000	85000
Load 4	79000	7218	7218	86218
Load 5	82000	7218	2000	84000

Table 4.2: Loads for evaluation of tension limit in commercial software.

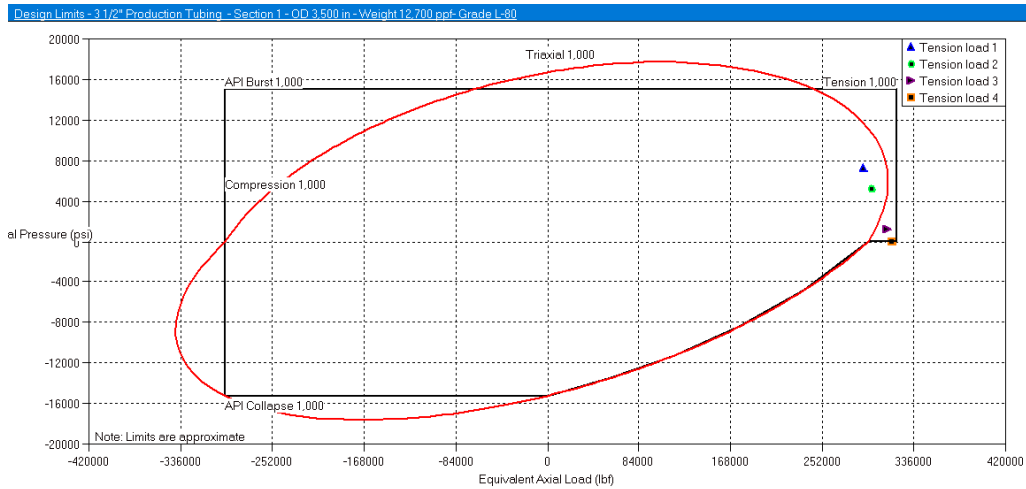


Figure 4.4: Design limits plot from commercial software for loads with safe axial tension force.

The loads are evaluated for 100 ft of pipe to generate only one point per case, making it easier to compare them. All the loads in figure 4.4 have axial stress lower than the yield strength and are therefore shown to the left of the tension limit. This is achieved by moving the line to the right of its original value (80000 psi = 294524 lb) and makes the loads be presented as safe in terms of axial stress, even if they are outside of the ellipse.

Load 5 is unsafe as its axial stress is higher than the yield strength. Figure 4.5 shows the design limit plot including this new case. The line will adjust, leaving load 5 out of the safety limits. As the axial stress of this load is 2000 psi higher than the yield strength, the line will be shown that amount of units to the left of the load, but this will make the axial stresses in loads 3 and 4 look like they are above the yield strength, which is not true.

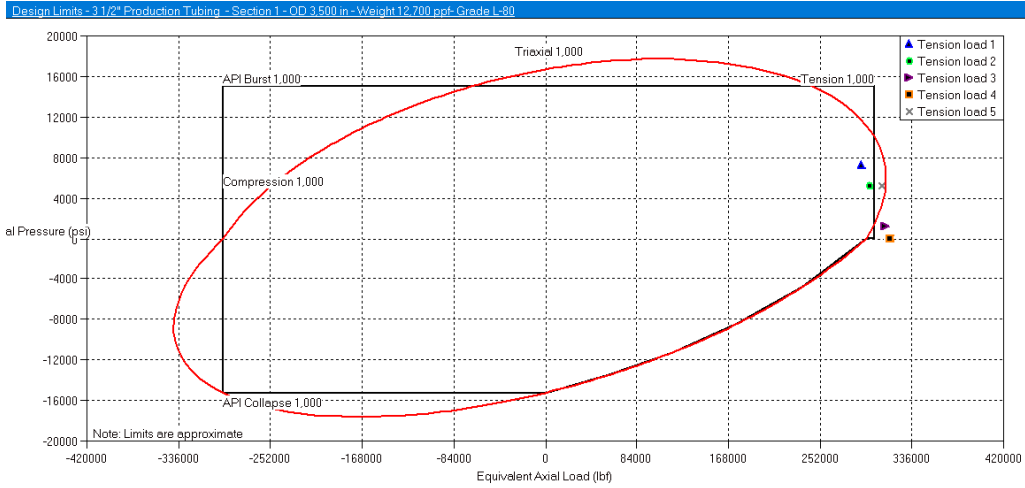


Figure 4.5: Design limit plot from commercial software including a load with unsafe axial force.

To do a similar evaluation for the compression limit in the left side of the plot, the loads in table 4.3 are used.

Cases	$\sigma_a$ (psi)	$p_i$ (psi)	$p_o$ (psi)	$\sigma_a + p_o$ (psi)
Load 1	-81000	7218	0	-81000
Load 2	-81000	7218	2000	-79000
Load 3	-81000	7218	6000	-75000
Load 4	-81000	7218	7218	-73782
Load 5	-79000	7218	2000	-77000

Table 4.3: Loads for evaluation of compression limit in commercial software.

Figure 4.6 is the plot for the cases 1 to 4. The line will move now the right to make sure that loads with unsafe axial stress ( $\sigma_a < -Y$ ) are outside the limit.

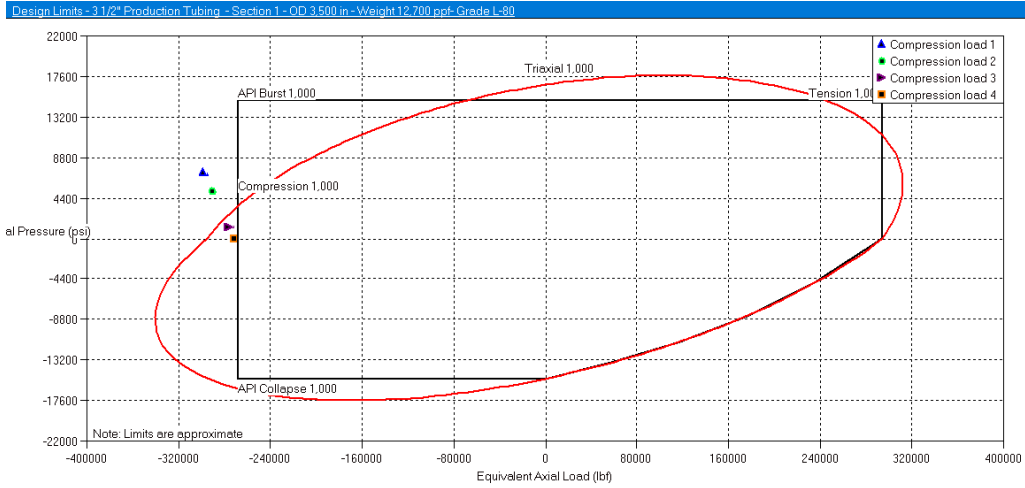


Figure 4.6: Design limit plot from commercial software for loads with safe axial compression stress and burst.

When including the load on case 5, for which the axial force is higher than the yield strength ( $\sigma_a > -Y$ ), the line will adjust again, moving to the left and including in the safe region some loads for which the axial stress will yield the pipe as observed in figure 4.7.

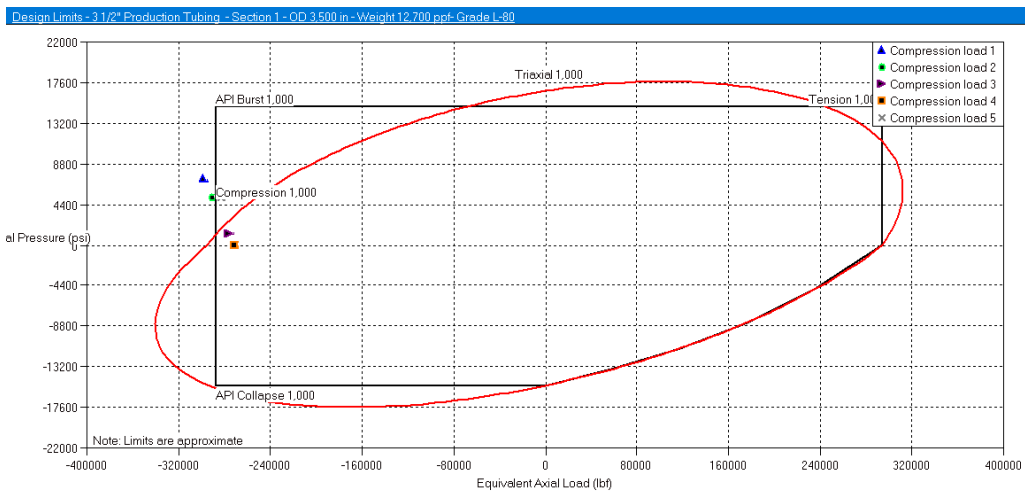


Figure 4.7: Design limit plot from commercial software including a load with unsafe axial stress and burst.

When plotting analogous cases corresponding to collapse loads, the same behavior is observed as showed in figures 4.8 and 4.9. In this case, the loads 6, 7 and 8 are unsafe and are initially presented outside the compression limit, however, when including load 9, which has safe axial stress, load 7 will be inside the safe region.

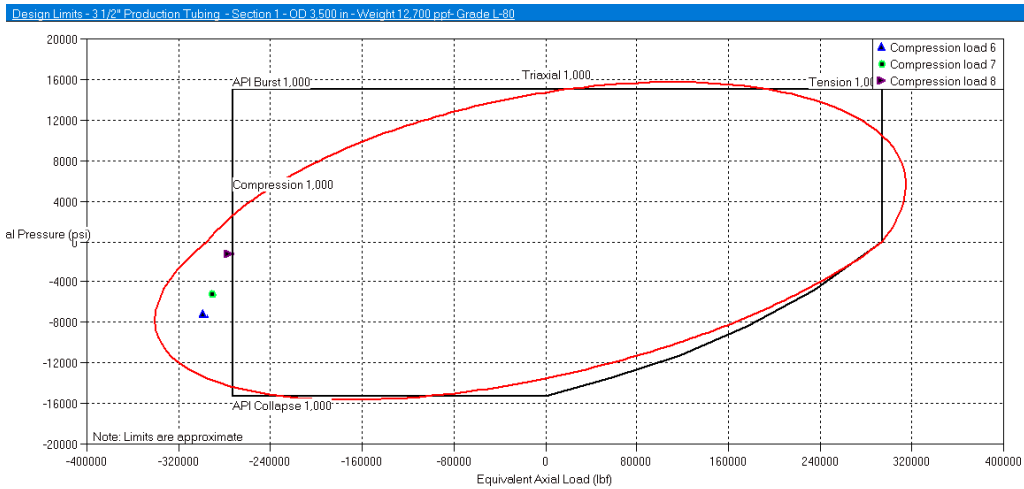


Figure 4.8: Design limit plot from commercial software including a load with unsafe axial stress and collapse.

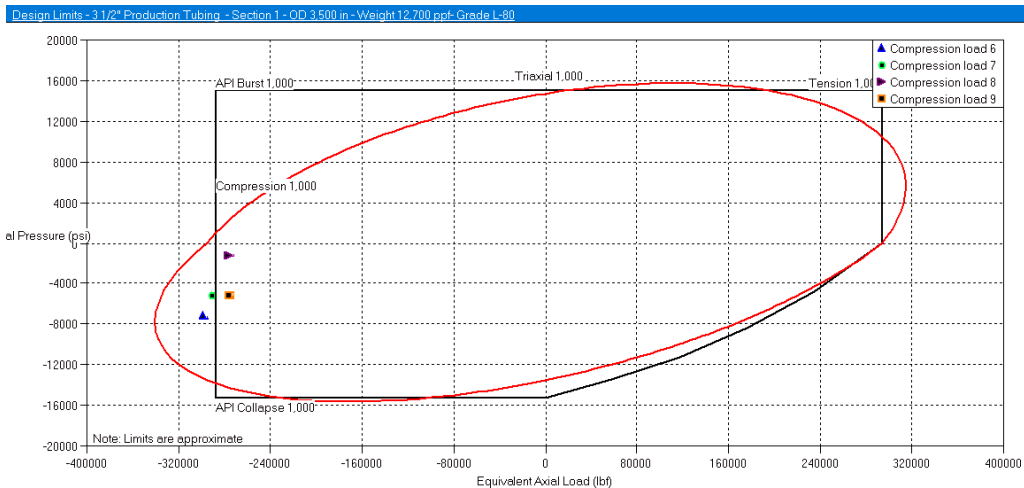


Figure 4.9: Design limit plot from commercial software including a load with unsafe axial stress and collapse.

A comparison of the plots in figures 4.4 and 4.5 with the ones in figures 4.6 and 4.7 shows that when no loads have a value of  $\sigma_a + p_o > Y$  the axial stress limit will be located at the value of the yield strength. The same is true for the compression line that will be located at the negative value of the yield strength.

The software approach is practical and can work well when evaluating a single load, however, for the presentation of several loads, it can lead to too conservative designs for the tension limit and unsafe designs for the compression limit. The last possibility is unacceptable as it can lead to well integrity issues.

In the plots from both approaches (Goodman et al. and the commercial software),



the horizontal lines corresponding to the burst and nominal collapse limit are not moved or adjusted in any case. This happens because the vertical axis has not been affected by the new API equation.

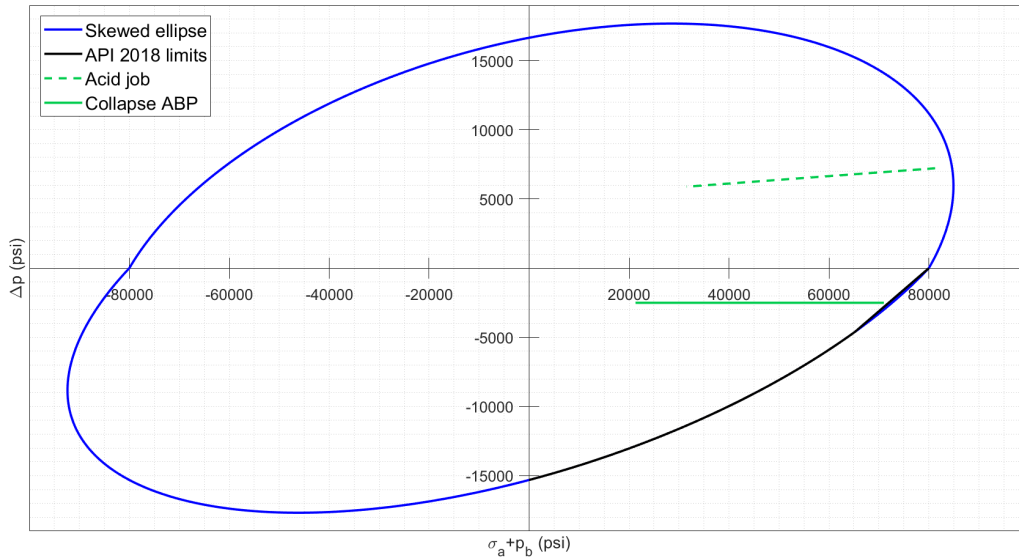
The standard API tension and compression limits, can not be accurately superimposed on either the commercial software or in the Goodman ellipse since they depend upon the load case. Therefore, the affirmation that the API limits can not be superimposed is not only true for the circle but also for the ellipse of plasticity. As a consequence, this common argument to prefer the use of the ellipse over the circle is disqualified.

### **4.3 Evaluation of new approaches**

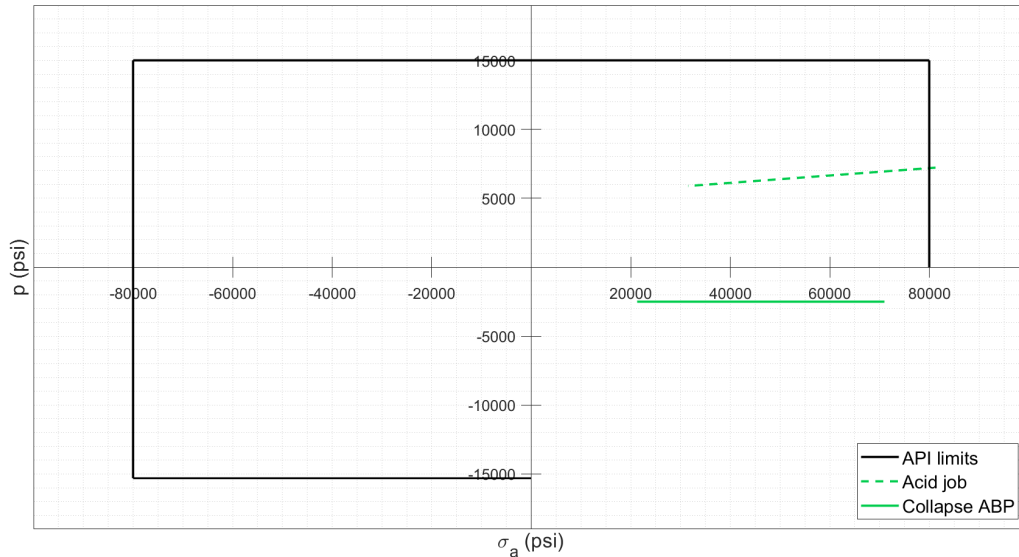
Three new alternatives are proposed for superimposing the API equations in the design limits plot.

#### **4.3.1 Separated plots**

To present results more accurately, the triaxial and uniaxial limits can be shown in separated plots. The example for the 3<sup>1</sup>/<sub>2</sub> in, 12.7 lb/ft, L80 pipe from Goodman et al., 2017, described in table 3.2 is presented in figure 4.10 using this approach.



(a) Triaxial limits.



(b) Uniaxial limits.

Figure 4.10: Ellipse of plasticity and API uniaxial limits with separated plots approach.

In both of the cases in the figure, the highest loads occur at the top of the pipe. For the acid job case, which corresponds to a burst situation,  $\sigma_a = 81255 \text{ psi}$ ,  $p_i = 7218 \text{ psi}$  and  $p_o = 0 \text{ psi}$ . The failure of the pipe is caused by the axial tension being higher than the yield strength as can be seen in figure 4.10b. For the annular pressure build-up, which corresponds to a collapse case, the highest load has  $\sigma_a = 70991 \text{ psi}$ ,  $p_i = 0 \text{ psi}$  and  $p_o = 2500 \text{ psi}$ . The plots presented in figure 4.10, provides clear information of which of the loads will lead to failure and which will be the failure mode. However, the fact that the information is split into two

plots and the need to correlate between them to determine how dangerous is the load makes them unpractical.

### 4.3.2 Slanted line

This option is based on the only points from the fixed vertical lines on the approach from Goodman et al. that have a real meaning, the points  $(Y, 0)$  and  $(-Y, 0)$ . Taking tension as example, the  $(Y, 0)$  coordinate is used as an initial position, and the limit will be plotted as a slanted line. To determine the slope of this line it is necessary to identify a load with axial stress higher than  $Y$  and that has the smallest  $\sigma_a + p_o$  (the closest unsafe load to  $Y$ ). The value  $x$ , in the abscissa, of the tension limit is determined by the difference between axial stress and the tensile strength ( $\sigma_a - Y$ ):

$$x = (\sigma_a + p_o) - (\sigma_a - Y) = p_o + Y$$

The coordinates of a point in the limit line with the same pressure differential of the load are  $(p_o + Y, p_i - p_o)$ . Having now two coordinates in the plane, the line can be plotted and then extended to the burst limit. To find the point where the tension line and the burst limit meet, it is necessary to refer to the equation of a line:

$$y = mx + b$$

Where  $m$  is the slope of the line and  $b$  the interception of the line with the vertical axis, defined as:

$$m = \frac{y_2 - y_1}{x_2 - x_1}$$

Thus, for the point of interest:

$$m = \frac{(p_i - p_o) - 0}{p_o + Y - Y} = \frac{(p_i - p_o)}{p_o}$$

Using the point  $(Y, 0)$  to find  $b$ :

$$0 = \frac{(p_i - p_o)}{p_o} Y + b$$

Therefore:

$$b = -\frac{(p_i - p_o)}{p_o} Y$$

The line equation is:

$$y = \frac{(p_i - p_o)}{p_o} (x - Y)$$

And the interception of the burst and tension lines is given by:

$$x = \left[ \frac{p_o}{(p_i - p_o)} \right] p_{burst} + Y$$

Or in terms of the variables used in the plot:

$$(\sigma_a + p_o)_{burst} = \left[ \frac{p_o(load)}{(p_i - p_o)_{load}} \right] p_{burst} + Y \quad (4.3)$$

Equation 4.3 indicates that the line is independent of the axial force and depends only on the pressures and some mechanical properties of the pipe. For the 3<sup>1</sup>/<sub>2</sub> in, 12.7 lb/ft, L80 pipe, when applying a load of  $\sigma_a = 810000 \text{ psi}$ ,  $p_i = 7000 \text{ psi}$  and  $p_o = 5000 \text{ psi}$ ; Using equation 4.3,  $\sigma_a + p_o$  will be:

$$(\sigma_a + p_o)_{burst} = \left[ \frac{5000}{(7000 - 5000)} \right] (15000) + 80000 = 117500 \text{ psi}$$

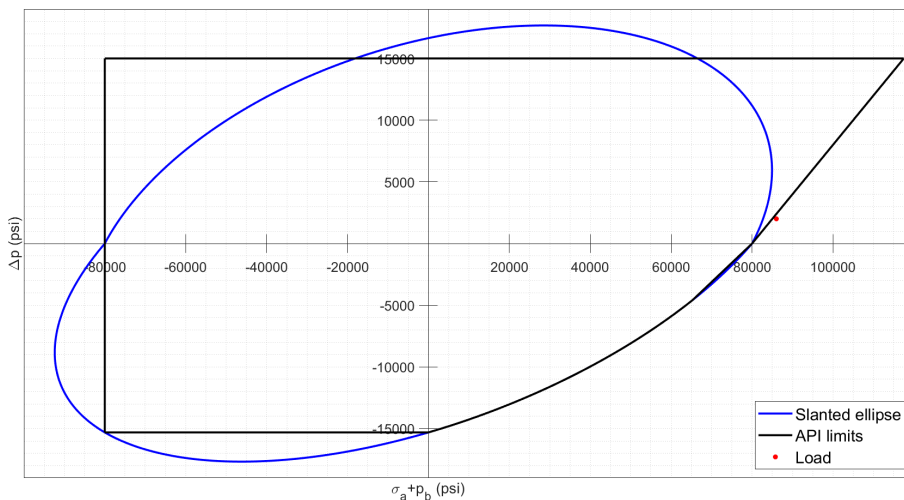


Figure 4.11: Ellipse of plasticity using the slanted line approach for an unsafe load.

In figure 4.11, the load is correctly located to the right of the line. When applying a load of  $\sigma_a = 79000 \text{ psi}$ ,  $p_i = 7000 \text{ psi}$  and  $p_o = 5000 \text{ psi}$  on the same pipe,  $\sigma_a + p_o$  will be  $117500 \text{ psi}$ , which is the same value obtained with the calculation for the unsafe load:

$$(\sigma_a + p_o)_{burst} = \left[ \frac{5000}{(7000 - 5000)} \right] (15000) + 80000 = 117500 \text{ psi}$$

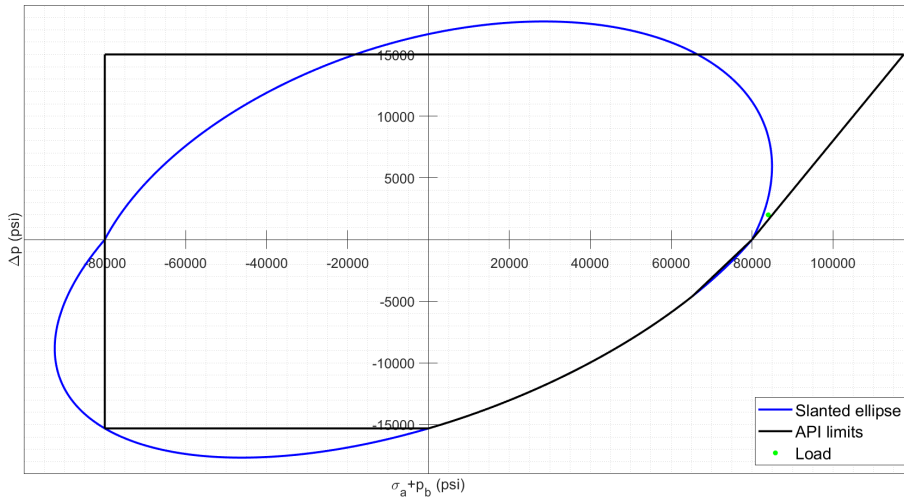


Figure 4.12: Ellipse of plasticity using the slanted line approach for a safe load.

In figure 4.12, the load is again located correctly, this time to the left of the line. The approach works well for both examples and is therefore convenient for plotting individual cases. When multiple loads need to be presented at the same time, the line will need to adjust to the unsafe load that has the lowest axial stress. This will cause some safe loads to appear to the right of the limit as happened with the vertical line in the commercial software approach and the method will not be so convenient.

### 4.3.3 Color scheme

A last proposed approach is not based on a visual comparison between the axial limit and the applied loads but the indication of unsafe loads through colors. The result is a plot that shows the ellipse of plasticity with the API limits excluding the axial compression and tension lines. Instead, when evaluating a load in terms of its axial stress, if safe, the load will be plotted in color green and when it is unsafe the color will be red. The result of using this approach for the burst case in table 3.2 is presented in figure 4.13.

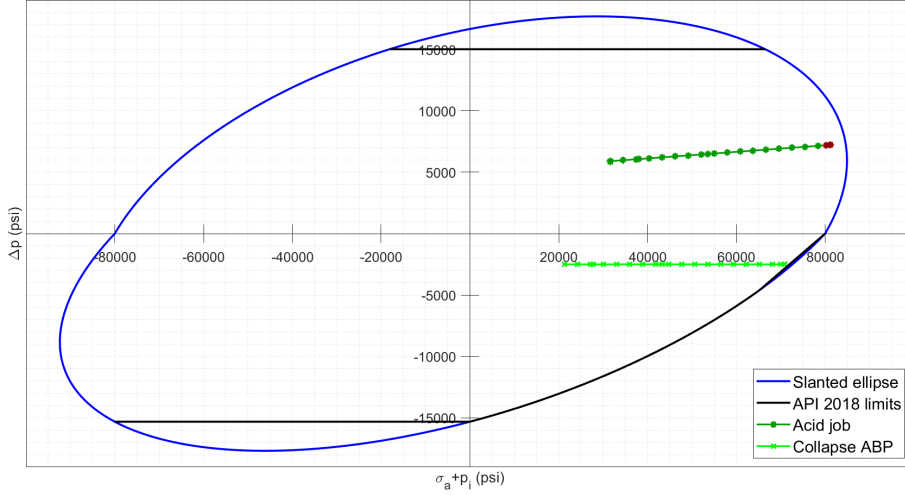


Figure 4.13: Ellipse of plasticity and API limits using color scheme.

The color scheme avoids the use of moving or slanted lines, or multiple plots and still indicates the existence of unsafe loads according to the API limits. In this case, all the loads are independently evaluated and therefore several cases can be presented in the same plot without interfering with each other. The approach is simple and intuitive, allowing to identify which load will cause the failure of pipe and the failure mode. Therefore this approach is the most convenient when presenting the design limits plot using the ellipse solving the incompatibility between the API triaxial and uniaxial limits. The next step is to evaluate these solutions in the circle of plasticity.

## 4.4 Implementation of circle plot

To call the attention to the circle and evaluate the proposed plotting methods, it is required to select the most convenient axis when working with it. Equation 2.17 uses  $\Delta\sigma_a$  as horizontal axis and  $\sqrt{3}\frac{D^2}{D^2-d^2}(p_i - p_o)$  as the vertical axis giving a circle shape. These values are not easy to handle, therefore some adjustments can be made to the equation to make it more practical. Using the geometrical factor in equation 2.19 and dividing by  $\frac{\sqrt{3}}{2}\beta$  the circle equation can be expressed as:

$$\Delta\sigma_a^2 + \left[ \frac{\sqrt{3}}{2}\beta (p_i - p_o) \right]^2 = Y^2$$

$$\Delta\sigma_a^2 + \frac{3}{4}\beta^2 (p_i - p_o)^2 = Y^2 \quad (4.4)$$

Equation 4.4 is the one of an horizontal ellipse of the form:

$$x^2 + \frac{3}{4}\beta^2 y^2 = Y^2$$

Where  $\Delta\sigma_a$  is the x-axis and  $(p_i - p_o)$  is the y-axis. This is very convenient as it allows to evaluate pressure changes independently of axial loads while the interaction between the fluid pressure and the axial force is still considered in the effective force. Thus, the effects of pressure changes can directly be observed. This selection of axes is extensible to evaluations of other types of pipes, for example, coiled tubing, as showed by McSpadden and Newman, 2002. A plot comparing the horizontal ellipse and the original slanted ellipse is presented in figure 4.14 (based on McSpadden and Newman, 2002 ).

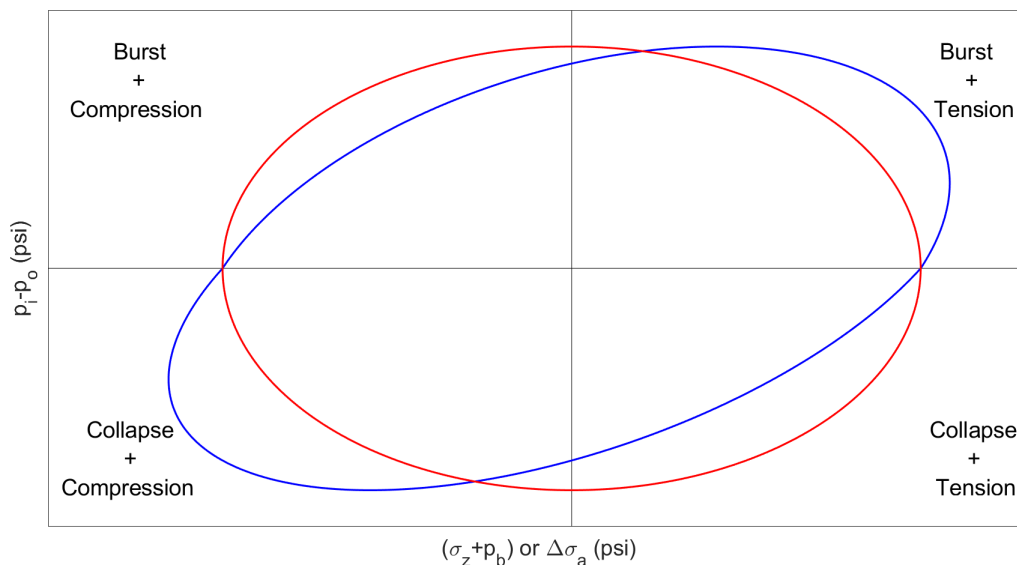


Figure 4.14: Comparison of slanted ellipse and circle of plasticity (expressed as an horizontal ellipse).

In this plot, a correspondence between the points of both ellipses is observed. Changing the datum from real to effective force, makes every pressure value in the slanted ellipse move a certain amount of units in the horizontal axis until the shape becomes symmetrical. This movement is to the left in the burst half of the plot and to the right in the collapse half. As the new formulation of the circle is also an ellipse, it will be called horizontal ellipse from now on, while the original skewed shape will be referred to as the slanted ellipse.

The slanted shape of the original ellipse may give the false indication that the pipe is strong in the quadrants corresponding to burst+tension and collapse+compression,

but weak in the quadrants of burst+compression and collapse+tension (Aasen et al., 2017). However, the horizontal ellipse clearly indicates that the pipe is equally strong under any combination of loads.

Aasen, 2007 used the expression for the neutral point derived by Woods (Klinkenberg, 1951) to define a neutral equilibrium line for a dimensionless slanted ellipse given by  $y = 2x$ . When adapted to the slanted ellipse used in this project it will be  $y = 2x/\beta$ . For the horizontal ellipse, the neutral equilibrium is defined by  $x = 0$ . To the left of the line, there is the “unstable region” in which the potential for buckling in the pipe exists. To the right of the line the pipe is stable (“stable region”). This neutral equilibrium equation for the slanted ellipse is only valid for the collapse half. To properly compare the two ellipses, it will be now defined for the burst half. Starting by the neutral point definition given by Woods (discussion in Klinkenberg, 1951):

$$\sigma_a = \frac{\sigma_h + \sigma_r}{2} \quad (4.5)$$

For burst and collapse in a vertical well, the pipe will fail at the inner wall where the hoop and radial stress formulations from the Lamé equation become  $\sigma_h = \beta(p_i - p_o) - p_i$  and  $\sigma_r = -p_i$ . Inserting them in equation 4.5:

$$\sigma_a = \frac{\beta(p_i - p_o) - p_i - p_i}{2}$$

$$2\sigma_a = \beta(p_i - p_o) - 2p_i$$

Adding  $2p_o$  on both sides:

$$2(\sigma_a + p_o) = \beta(p_i - p_o) - 2(p_i - p_o)$$

$$2(\sigma_a + p_o) = (\beta - 2)(p_i - p_o)$$

$$(p_i - p_o) = \frac{2(\sigma_a + p_o)}{\beta - 2}$$

$$y = \frac{2x}{\beta - 2} \quad (4.6)$$



Equation 4.6 defines the neutral equilibrium line for the burst half of the ellipse and having a different slope than the equation for the collapse half it fits to the results from Goodman et al., 2017. Both ellipses with their respective neutral equilibrium lines and are presented in figure 4.15.

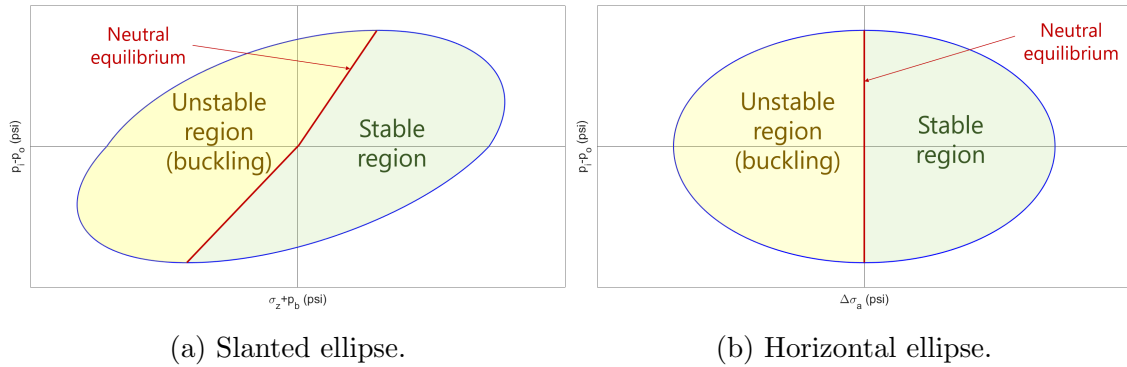


Figure 4.15: Neutral equilibrium in slanted and horizontal ellipses for a pipe with  $\beta = 7.1673$  and  $D/t = 13.2530$ .

Due to its symmetry, in the horizontal ellipse, the neutral equilibrium appears as a single line overlapping the vertical axis. This makes this ellipse simpler to build and the distinction between the two regions is more intuitive. The slanted ellipse is not usually plotted with the neutral equilibrium line, so the standard plot does not give meaningful information about buckling potential in the pipe.

McSpadden and Newman, 2002 demonstrated that the use of effective force is practical as it allows to directly use the surface weight in the plot. This is a parameter usually measured in operations and has the same value as the effective force.

The use of the horizontal ellipse is, therefore, the most convenient: it is simpler than the slanted ellipse but still easy to relate to it. Due to its axes, the horizontal ellipse is compatible with other analyses made on pipes as buckling (it is important to remember that collapse is a problem of wall buckling in pipes), making it more practical for drilling and completion engineers.

## 4.5 API collapse equation in neutral stress datum

Once the axes of the plot have been defined, the API triaxial collapse limit can be adapted to it. Starting from equations 2.14 and 2.15:

$$\Delta\sigma_a = \sigma_a - \sigma_n = \sigma_a - \frac{d^2 p_i - D^2 p_o}{D^2 - d^2}$$

$$\Delta\sigma_a = \sigma_a - \frac{d^2 p_i - D^2 p_o}{D^2 - d^2} + p_i - p_i$$

$$\Delta\sigma_a = (\sigma_a + p_i) - \frac{d^2 p_i - D^2 p_o}{D^2 - d^2} - p_i$$

$$\Delta\sigma_a = (\sigma_a + p_i) - \frac{d^2 p_i}{D^2 - d^2} + \frac{D^2 p_o}{D^2 - d^2} - p_i \frac{(D^2 - d^2)}{(D^2 - d^2)}$$

$$\Delta\sigma_a = (\sigma_a + p_i) - \frac{p_i}{D^2 - d^2} (d^2 + D^2 - d^2) + \frac{D^2 p_o}{D^2 - d^2}$$

$$\Delta\sigma_a = (\sigma_a + p_i) - \frac{D^2}{D^2 - d^2} (p_i - p_o)$$

From the definition of  $\beta$ :

$$\Delta\sigma_a = (\sigma_a + p_i) - \frac{1}{2}\beta (p_i - p_o) \quad (y < 0) \quad (4.7)$$

Equation 4.7, presents a first relation between the two shapes in which the independent variable is  $\sigma_a + p_i$  and therefore is valid only for the collapse half of the ellipse (when  $p_i - p_o < 0$ ). When applying a similar derivation but adding and subtracting  $p_o$ , the analogous equation for the burst half of the plot (when  $p_i - p_o > 0$ ) can be obtained as presented in equation 4.8. A detailed derivation of this equation is found in the appendix B. This follows the methodology used by Goodman et al., 2017 who developed an equation for each half of the ellipse which now corresponds with the two equations to relate the slanted and horizontal ellipse.

$$\Delta\sigma_a = (\sigma_a + p_o) - \frac{1}{2}k\beta(p_i - p_o) \quad (y > 0) \quad (4.8)$$

The API collapse equations calculate the collapse pressure under zero axial stress datum, this is, as a function of  $\sigma_a + p_i$ . To include those results in the neutral axial stress horizontal ellipse, it is necessary to use the value of the collapse pressure to calculate the available effective force. Equation 4.7, can be re arranged to obtain  $\sigma_a + p_i$ :

$$\sigma_a + p_i = \Delta\sigma_a + \frac{1}{2}\beta(p_i - p_o) \quad (4.9)$$

Replacing equation 4.9 in API equation 42 (API, 2018):

$$Y_* = \sqrt{Y^2 - \frac{3}{4} \left[ \Delta\sigma_a + \frac{1}{2}\beta(p_i - p_o) \right]^2} - \frac{1}{2} \left[ \Delta\sigma_a + \frac{1}{2}\beta(p_i - p_o) \right]$$

Multiplying by 2 on both sides:

$$2Y_* = \sqrt{4Y^2 - 3 \left[ \Delta\sigma_a + \frac{1}{2}\beta(p_i - p_o) \right]^2} - \Delta\sigma_a - \frac{1}{2}\beta(p_i - p_o)$$

$$\left[ \Delta\sigma_a + \frac{1}{2}\beta(p_i - p_o) + 2Y_* \right]^2 = 4Y^2 - 3 \left[ \Delta\sigma_a + \frac{1}{2}\beta(p_i - p_o) \right]^2$$

Extending the polynomials:

$$\begin{aligned} \Delta\sigma_a^2 + \beta(p_i - p_o) \Delta\sigma_a + 4Y_* \Delta\sigma_a + \frac{1}{4}\beta^2(p_i - p_o)^2 + 2\beta(p_i - p_o) Y_* + 4Y_*^2 \\ = 4Y^2 - 3\Delta\sigma_a^2 - 3\beta\Delta\sigma_a(p_i - p_o) - \frac{3}{4}\beta^2(p_i - p_o)^2 \end{aligned}$$

$$4\Delta\sigma_a^2 + [4\beta(p_i - p_o) + 4Y_*] \Delta\sigma_a + \beta^2(p_i - p_o)^2 + 2\beta(p_i - p_o) Y_* + 4Y_*^2 - 4Y^2 = 0$$

This expression is a quadratic equation of the form  $ax^2 + bx + c = 0$ , where:

$$x = \Delta\sigma_a$$

$$a = 4$$

$$b = 4\beta(p_i - p_o) + 4Y_*$$

$$c = \beta^2(p_i - p_o)^2 + 2\beta(p_i - p_o) Y_* + 4Y_*^2 - 4Y^2$$

It can be therefore solved using the quadratic formula, where:

$$b^2 = 16\beta^2(p_i - p_o)^2 + 32\beta^2(p_i - p_o) Y_* + 16\beta^2 Y_*^2$$

$$4ac = 16\beta^2 (p_i - p_o)^2 + 32\beta^2 (p_i - p_o) Y_* + 64Y_*^2 - 64Y^2$$

Therefore:

$$\Delta\sigma_a = \frac{-4\beta (p_i - p_o) - 4Y_* \pm \sqrt{64Y^2 - 48Y_*^2}}{8}$$

Taking the positive sign and simplifying:

$$\Delta\sigma_a = \sqrt{Y^2 - \frac{3}{4}Y_*^2} - \frac{Y_*}{2} - \frac{1}{2}\beta (p_i - p_o) \quad (4.10)$$

Or:

$$(p_i - p_o) = \frac{1}{\beta} \left( \sqrt{4Y^2 - 3Y_*^2} - Y_* - 2\Delta\sigma_a \right) \quad (4.11)$$

Equations 4.10 and 4.11 are convenient as they use only values calculated from API formulas in order to evaluate the available pressure differential or effective axial stress. In other words, they correspond to the API equations in terms of a neutral stress datum.

## 4.6 Superimposition of API collapse equation in the horizontal ellipse plot

The API equations are derived from pressure tests under zero axial datum conditions, as a consequence, their results are representative of those conditions. It is, therefore, necessary to first calculate the collapse pressures differential using API equations and then use these values to find the corresponding effective force using equation 4.10. The API equations are valid only for  $\sigma + p_o \geq 0$  *psi* and  $Y_* < 24000$  *psi* and therefore the right range for the curve must be chosen. Inserting the first condition in equation 4.7:

$$\Delta\sigma_a = 0 + \frac{1}{2}\beta p_c = \frac{\beta}{2}p_c$$

As in collapse  $p_i < p_o$  the negative sign is converted into a positive sign when the nominal collapse pressure is replaced. Therefore, the domain of the curve will go from  $\frac{\beta}{2}p_c$  to the effective force calculated from the pressure value when  $Y_* = 24000 \text{ psi}$  using equation 4.10.

## 4.7 Superimposition of API axial limits in the horizontal ellipse

The methodology to superimpose the triaxial collapse limit in the horizontal ellipse has been presented, it is necessary now to select an approach to include the uniaxial limits. The burst and nominal collapse limits are not affected by the change in the horizontal axis, therefore, the horizontal lines that represent them are not changed. The vertical lines corresponding to axial compression and tension limits are however affected and need to be adjusted.

The same analysis and conclusions obtained for the approaches from Goodman et al., 2017 and the commercial software in the slanted ellipse are valid for the horizontal one. In the case of the fixed vertical lines, the result shown in figure 4.16 can be expected.

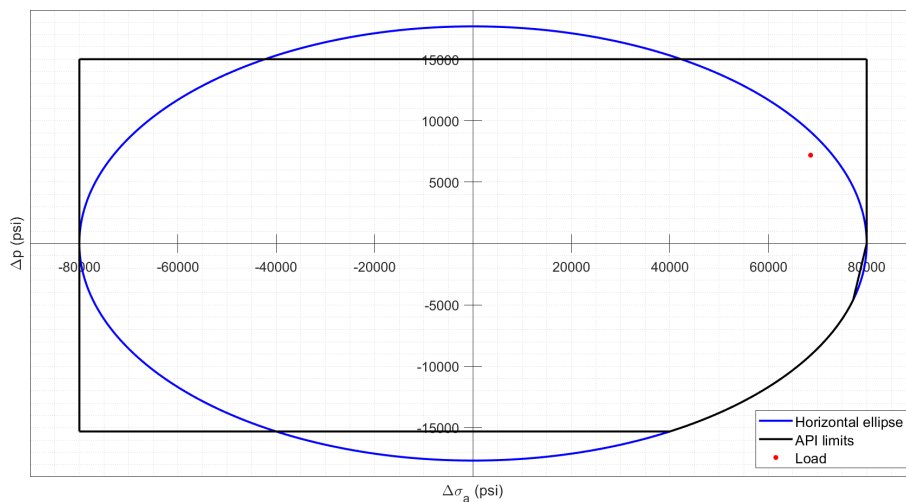


Figure 4.16: Application of the approach from Goodman et al. to the horizontal ellipse.

The red point in the figure is a load with axial stress slightly higher than the yield strength ( $\sigma_a = 80013 \text{ psi}$ ,  $p_i = 7377 \text{ psi}$ ,  $p_o = 187 \text{ psi}$  and  $\Delta\sigma_a = 68600 \text{ psi}$ ). This load is in the safe region due to the influence of the internal and external pressures

on the effective force. As in the slanted ellipse, the fixed-line is valid, only for loads in which  $p_i = p_o = 0$ . Otherwise, the approach will give inaccurate results.

When applying the algorithm from the commercial software, to move the vertical line according to the load, the horizontal ellipse plot will look like figure 4.17.

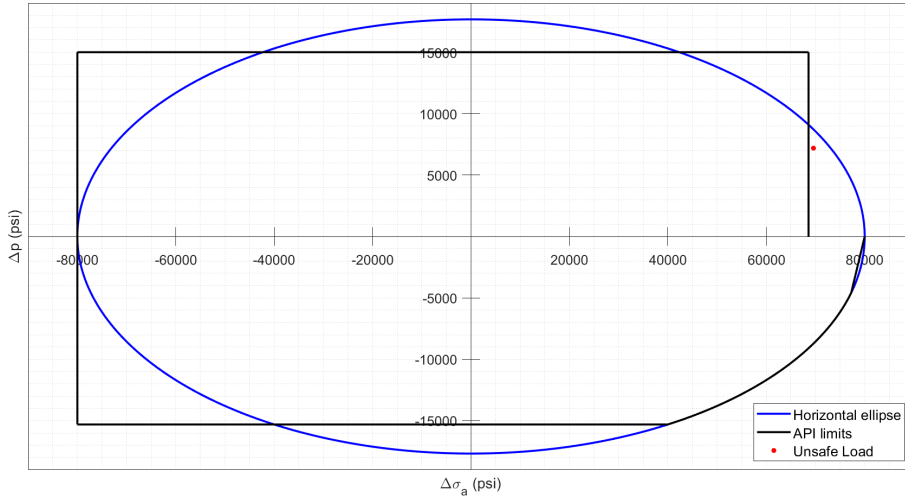


Figure 4.17: Application of the same approach as the commercial software to the horizontal ellipse.

In this case, the unsafe load are correctly presented outside of the limit, but the shift of the line to the left gives the impression of a lower yield strength and a narrower safe region. This leads to a misconception of the tension limit. The weaknesses of this approach in the slanted ellipse are transferable to the horizontal ellipse and therefore when presenting multiple loads at the same time, some of the safe ones can be presented to the left of the line.

#### 4.7.1 Slanted line in horizontal ellipse

The first of the new approaches to present the API axial limits to be tested in the horizontal ellipse is the one that uses slanting lines.

##### Derivation of the line equation

As mention previously, the only point that has a real meaning in the vertical line of the slanted ellipse is the point  $(Y,0)$  and the same is true for the horizontal ellipse, thus, it will be used as a starting point for the line. Then, the tension limit will be plotted as a slanted line. To determine the slope it is necessary to identify a load

with axial stress higher than  $Y$  and that has the smallest effective stress (the closest unsafe load to  $Y$ ). This time, the coordinate of the load in the x-axis is given by the definition of effective force from equation 2.16 written in terms of stress:

$$\Delta\sigma_a = \sigma_a + \frac{A_o}{A_s}p_o - \frac{A_i}{A_s}p_i$$

The tension limit must be adjusted to this load to make sure it will be out of the safe region. The value  $x$  in the abscissa of the tension limit is determined by the difference between axial stress and the tensile strength ( $\sigma_a - Y$ ):

$$x = \Delta\sigma_a - (\sigma_a - Y)$$

By the definition of effective force:

$$x = \sigma_a + \frac{A_o}{A_s}p_o - \frac{A_i}{A_s}p_i - \sigma_a + Y$$

$$x = Y + \frac{A_o}{A_s}p_o - \frac{A_i}{A_s}p_i$$

Therefore, the coordinates of a point in the limit that has the same pressure differential of the load will be  $\left(Y + \frac{A_o}{A_s}p_o - \frac{A_i}{A_s}p_i, (p_i - p_o)\right)$ . Having now two coordinates in the plane, the line can be plotted and then extend it to the burst limit. To find the point where the tension line and the burst limit meet, it is necessary to refer to the equation of a line:  $y = mx + b$ . Calculating the slope  $m$ :

$$m = \frac{y_2 - y_1}{x_2 - x_1}$$

$$m = \frac{(p_i - p_o) - 0}{Y + \frac{A_o}{A_s}p_o - \frac{A_i}{A_s}p_i - Y}$$

$$m = \frac{A_s(p_i - p_o)}{A_o p_o - A_i p_i}$$

And the line equation becomes:

$$y = \frac{A_s(p_i - p_o)}{A_o p_o - A_i p_i}x + b$$

Using the point  $(Y, 0)$  to find  $b$ :

$$0 = \frac{A_s (p_i - p_o)}{A_o p_o - A_i p_i} Y + b$$

Therefore:

$$b = -\frac{A_s (p_i - p_o)}{A_o p_o - A_i p_i} Y$$

And the definitive line equation is:

$$y = \frac{A_s (p_i - p_o)}{A_o p_o - A_i p_i} (x - Y)$$

The interception of the burst and tension lines is give by:

$$x = \left[ \frac{A_o p_o - A_i p_i}{A_s (p_i - p_o)} \right] p_{burst} + Y$$

Or in terms of the variables in use in the plot:

$$\Delta\sigma_{a(burst)} = \left[ \frac{A_o p_{o(load)} - A_i p_{i(load)}}{A_s (p_i - p_o)_{load}} \right] p_{burst} + Y \quad (4.12)$$

$p_i$  and  $p_o$  in this equation are the internal and external pressure of the load with axial stress higher than  $Y$  and that has the smallest effective stress. Equation 4.12 is only applicable when there are loads with effective force higher than the yield ( $\Delta\sigma_a > Y$ ) strength and for which the internal and external pressures are different.

### Example

Some for the loads from the burst case for the 3<sup>1/2</sup> in, 12.7 lb/ft, L80 pipe in Goodman et al., 2017 are presented in the next table:



Load	$\sigma_a$ (psi)	$p_i$ (psi)	$p_o$ (psi)	$\Delta p$ (psi)	$\sigma_a + p_i$ (psi)	$\Delta\sigma_a$ (psi)
1	81080	7240	26	7214	81106	69467
2	81010	7249	37	7212	81047	69412
3	80013	7377	187	7190	80200	68600
4	77944	7642	499	7243	78443	66919
5	74494	8083	1018	7065	75512	64114

The load with axial stress higher than the yield strength and that has the smallest effective force is 3. Using equation 4.12:

$$\Delta\sigma_{a(burst)} = \left[ \frac{(9.6211)(187) - (5.9396)(7377)}{(3.6816)(7190)} \right] (15000) + 80000 = 56530 \text{ psi}$$

Then, the coordinates of the point where the burst pressure and the axial tension lines meet are (56530,15000) and the resulting plot is presented in figure 4.18.

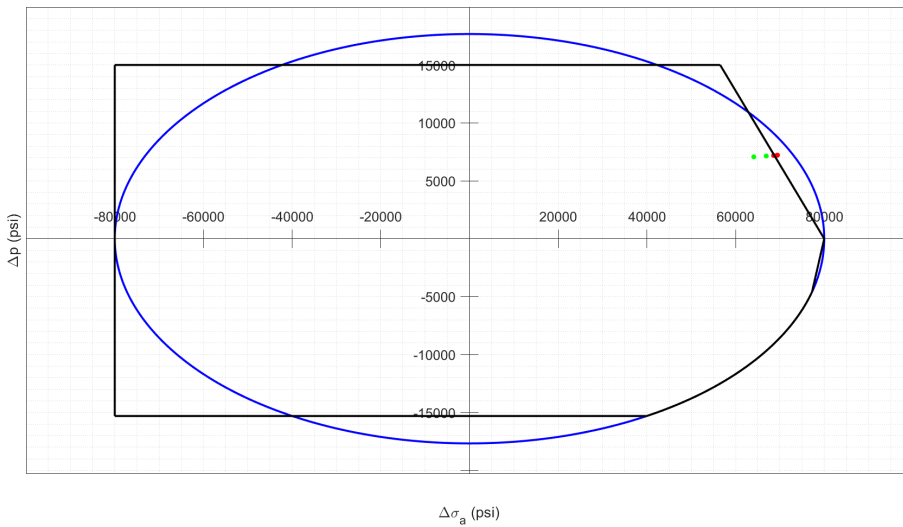


Figure 4.18: API limit superimposed in the horizontal ellipse using the slanted line approach.

The slanted line in this figure goes very close to load 3, this is expected, as the axial force is just 13 psi higher than the yield strength but the dangerous loads (in red) are outside the limit. The value of the yield strength is determined in the figure as the interception of the tension limit line with the horizontal axis. The plot is consistent with the adjustment of the slanted ellipse into a horizontal one. As discussed previously, it is done by moving all the values in the limit above (Y, 0) to the left in the horizontal axis. As the formula presented in equation 4.12 depends

on the internal and external pressure of the load, any change made on them will lead to an adjustment of the line. If plotting simultaneous loads, all the unsafe ones will be out of the safe region.

### Safe loads

The approach of a slanted line is weak in the horizontal ellipse when a load with axial stress lower than the yield strength ( $\Delta\sigma_a < Y$ ) and  $p_o = p_i \neq 0$  for which the values of pressures are high. Taking as an example the 3<sup>1</sup>/<sub>2</sub> in, 12.7 lb/ft, L80 pipe used before and applying a load with  $\sigma_a = 79000 \text{ psi}$  and  $p_i = p_o = 7000 \text{ psi}$ ,  $\Delta\sigma_a$  will be  $86000 \text{ psi}$ . The resulting plot is presented in figure 4.19.

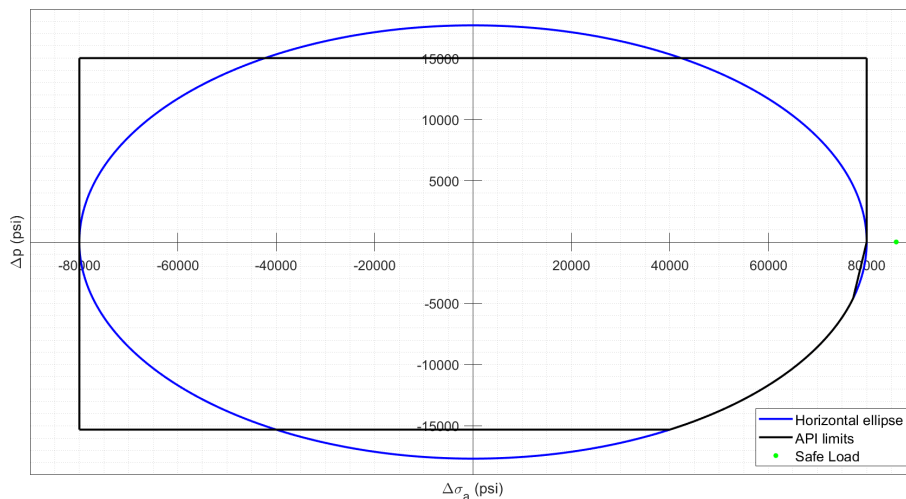


Figure 4.19: Slanted line approach for a load with equal internal and external pressures.

As the interception of the limit with the abscissa is fixed, not even tilting the line to the right will make the load be in the safe region. In the slanted ellipse an increase in the external pressure will shift the load to the left in the plot, but it will be compensated by a movement down in the vertical axis and the load will remain inside the tension limit. In the horizontal ellipse the movement to the left when there is a higher external pressure will be amplified by the external cross-sectional area according to the definition of the effective force and the movement down will not be able to compensate for it, making the load appear out of the limit. Therefore, the approach will be limited to loads that fulfill the condition of  $p_i = p_o \neq 0$ .

## 4.7.2 Color scheme approach in the horizontal ellipse

When applying the color scheme to the horizontal line, the result presents all the benefits as when applied to the slanted ellipse: it is simple, presents the information from all API limits in a single plot, and indicates the kind of failure mode that the pipe will present. When using this approach on the 3<sup>1</sup>/<sub>2</sub> in, 12.7 lb/ft, L80 pipe given as example, figure 4.20 is obtained. As in the skewed ellipse, the green color indicates safe loads and the red color unsafe loads.

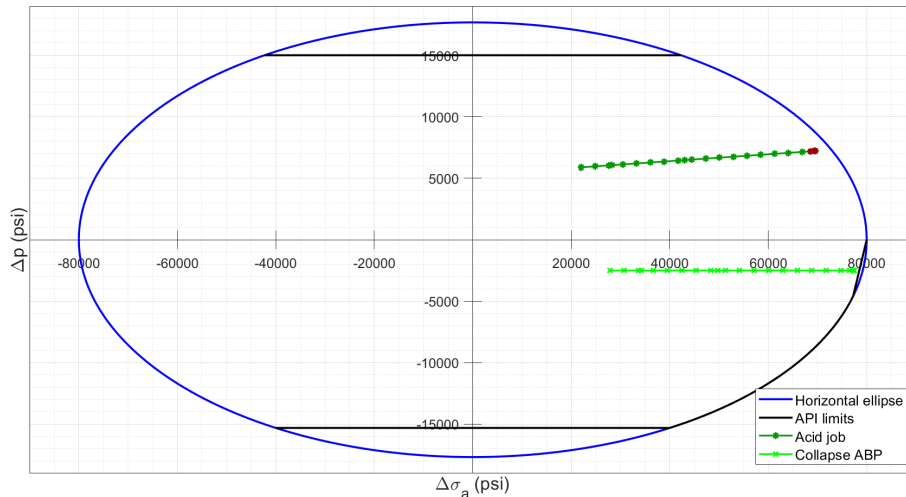


Figure 4.20: Color scheme approach in the horizontal ellipse.

As mentioned, one of the benefits of this approach is that multiple cases can be presented at the same time without interfering with each other as shown in figure 4.21, in which the safe and unsafe loads are indicated even if the limit line is not present.

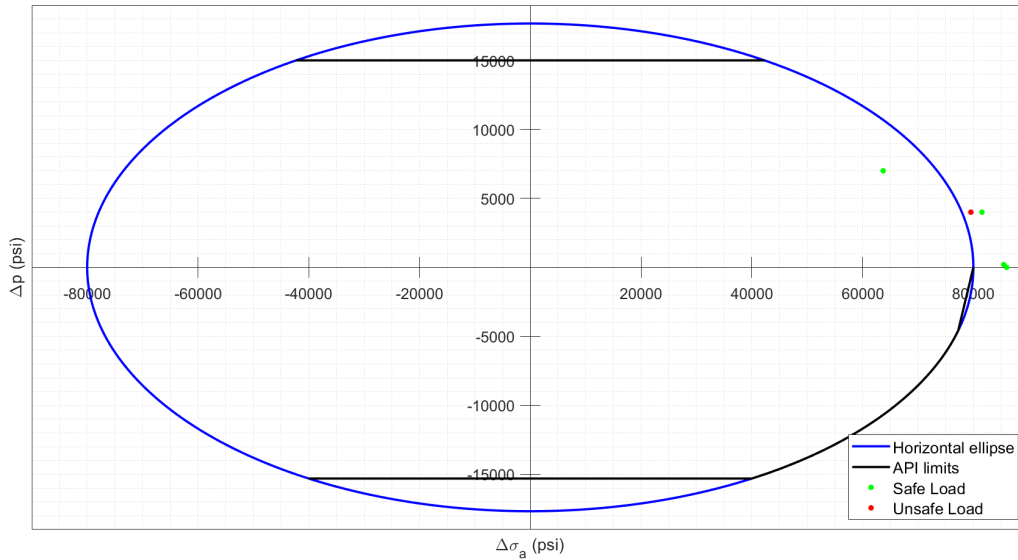


Figure 4.21: Color scheme applied to the horizontal ellipse when multiple loads are included.

## 4.8 New case

To highlight the convenience of the adapted horizontal ellipse and the new method of superimposing the API limits, a new case is presented. The example uses a vertical well in an HPHT reservoir, based on the design from the Elgin and Franklin fields in the North Sea described in Humphreys, 2000. The total depth is 19030 ft, with a water depth of 305 ft, an air gap of 100 ft, and a wellhead elevation of 60 ft from the Mean Sea Level. The initial temperature gradient involves 60°F at the wellhead, 40°F at the mudline, and 370°F at 19030 ft. The information about casings and tubing is presented in table 4.4 and the load cases in table 4.5. The tubing specifications are chosen to allow comparison between the plots when the simulated loads exceed the API limits, as observed in figures 4.22 to 4.23. The plot of the slanted ellipse using the Goodman et al. approach is included to compare the neutral equilibrium and the stable and unstable regions in the slanted and horizontal ellipses.

Pipe	Measured depth (ft)			Hole size (in)
	Hanger	TOC	Shoe	
30 in, 309.7 lb/ft, X56	40	405	730	36
20 in, 133 lb/ft, K55	40	405	2950	26
13 <sup>3</sup> / <sub>8</sub> in, 72 lb/ft, P110	6900	6100	11810	17 <sup>1</sup> / <sub>2</sub>
9 <sup>5</sup> / <sub>8</sub> in, 53.5 lb/ft, Q125	40	9100	16750	12 <sup>1</sup> / <sub>4</sub>
7 in, 42.7 lb/ft, T95 Liner	16300	16300	1930	8 <sup>1</sup> / <sub>2</sub>
5 <sup>1</sup> / <sub>2</sub> in, 23 lb/ft, N80	40		18800	

Table 4.4: Well design for new load case example.

Case	Load	Load description		
		$p_i$ (psi)	$p_o$ (psi)	Temperature
1	Injection	7000 psi @ 40 ft and 14980 psi @ 18800 ft	1000 psi on top of 17.2 ppg brine to 18800 ft	Fluid temp: 50°F Tubing temperature: 50 °F @ 40 ft ft and 79°F @18800 ft
2	Acid job	7000 psi @ 40 ft and 15935 psi at 18800 ft	17.2 ppg brine to 18800 ft	Fluid temp: 60°F Tubing temperature: 60 °F @ 40 ft ft and 81°F @18800 ft
3	Production	12500 psi @ 40 ft 16897 psi at 18800 ft	17.2 ppg brine to 18800 ft	333 °F @ 40 ft ft and 371°F @18800 ft
4	Tubing leak	12500 psi @ 40ft 16898 psi @ 18800 ft (from production case)	12500 psi on top of 17.2 ppg brine to 18800 ft	333 °F @ 40 ft ft and 371°F @18800 ft
5	APB	0 psi @ 40ft 16760 psi @ 18800 ft	7000 psi @ 40 ft 23760 psi at 18800 ft	60 °F @ 40 ft ft and 100°F @18800 ft

Table 4.5: Load cases for 5<sup>1</sup>/<sub>2</sub> in, 23 lb/ft, N80 pipe example.

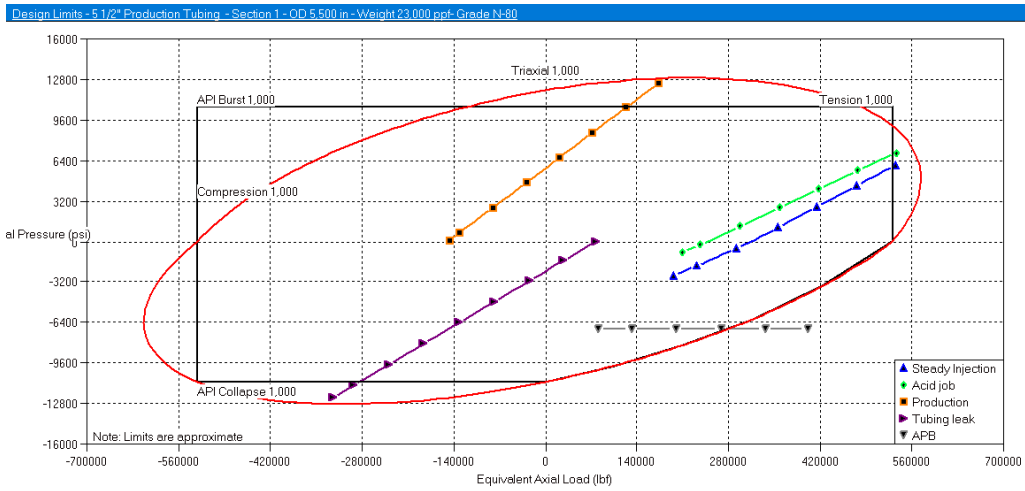


Figure 4.22: Plot from commercial software for the new case.

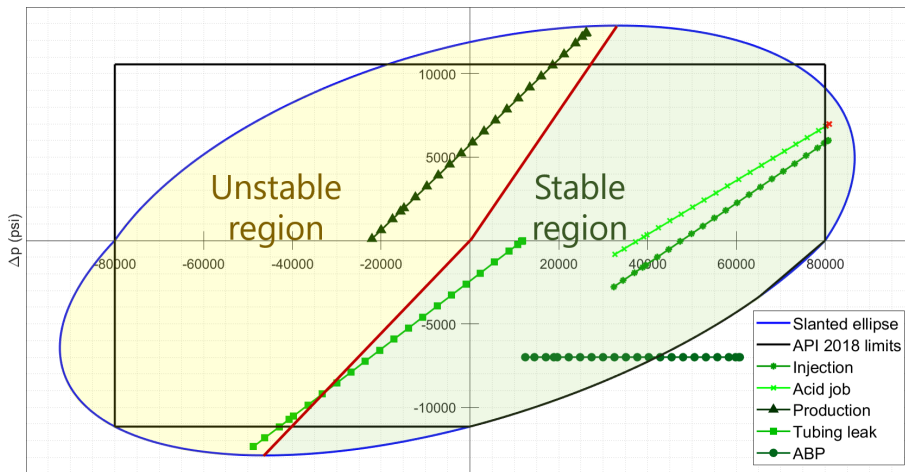


Figure 4.23: Plot using Goodman et al. approach in slanted ellipse for the new case.

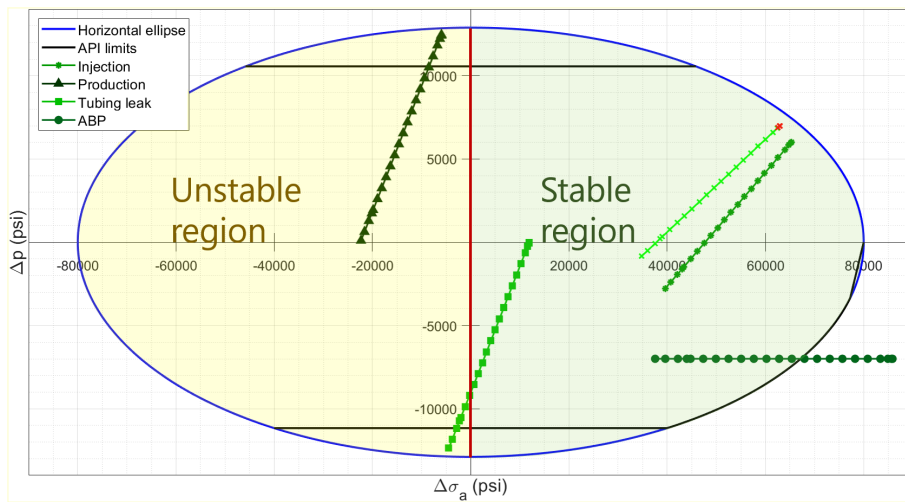


Figure 4.24: Plot using horizontal ellipse with the colors scheme for the new case.

The first case to be discussed is the steady injection of a fluid into the reservoir. In this situation, the tubing temperature will decrease due to the heat transfer to the cold injection fluid, reducing the pipe length and creating tension. The case line in the commercial software plot indicates failure due to axial stress. A similar behavior is observed for the case of an acid job. However, the data from calculations indicate that, for the injection case, the maximum axial force is 528669 lbs ( $\sigma_a = 79743$  psi). This force occurs at the top of the string and is below the tension limit, therefore, the pipe will be safe. Figure 4.22, however, indicates the opposite. In the acid job, the axial force at the top of the pipe is 537064 psi ( $\sigma_a = 81010$  psi), which will cause the failure of the pipe. If all other cases felt within the API limits, based in figure 4.24 an engineer will decide for a tubing with higher specifications, leading to higher costs in the well.

On the other hand, in figure 4.24, the completely green line in the steady injection case indicates that the axial loads are safe all along the pipe. The red section in the acid job line, instead, shows that the load at the top of the pipe will lead to failure. An acid job is an operation for which the parameters can be easily changed to adjust for the well features. If the main duty of the well is to be an injector, the injection parameters are chosen looking for the best reservoir performance and the well is the one which should adjust to these requirements. Figure 4.24 therefore, gives more accurate information to select the right tubing.

The third case corresponds to production of sour gas that given the high temperature and pressure in the reservoir, will lead to pipe failure. This failure mode will be burst and all three figures show this information clearly. The fourth case is a tubing leak during production of gas. The failure mode, in this case, is collapse, as noticed in the load line in figures 4.22 to 4.24 crossing the horizontal collapse limit. For cases 3 and 4, all figures give accurate information about the failure mode and pressure, due to the independence of the API burst and nominal collapse limits from the load case.

The production case is the worst-case scenario for axial compression and still, it is far from the vertical line to the left of the plot. The compression force is caused by the increase of the temperature of the pipe due to energy transferred from the produced fluid, leading to thermal expansion restricted by the production packer. The reason why the case line is far from the compression limit is that, for a vertical well, the tubing is naturally in tension when installed as its weight will exert axial tension force on the top of the string.

The last case to be discussed is the annular pressure build-up (APB). According

to the commercial software plot, the pipe will fail, due to collapse. The horizontal ellipse plot shows the same result. Even if the case line extends beyond 80000 psi the green color clearly indicates that the failure is not due to tension.

All lines in the plot are straight. This happens because API does not consider the effect of buckling in the pipe when evaluating axial force (in a real situation buckling will lead to failure before reaching the compression limit). It is, therefore, necessary to include buckling restrictions in the tubing to make sure that axial forces will lead to compression forces and not to buckling, contributing to the worst-case scenario. Keeping in mind that situation, the conclusion is that due to the tension state created on the tubing during its installation, even if no buckling is allowed, the pipe will never fail by axial compression. This statement is true for vertical wells. For deviated wells, some of the assumptions made for the horizontal ellipse must be changed (the stress will not be higher in the inner wall of the pipe for example). This is discussed in Aasen et al., 2017, however, for being out of the scope of this project, no more details are included in the present discussion. When comparing figures 4.23 and 4.24 in terms of buckling and the neutral equilibrium line, the results are the same, the loads in tension are shown in the “stable region” and the loads in compression in the “unstable region” for both cases. The section of the tubing leak line that presents the potential of buckling is the same in both plots and the section that is safe as well.

Failure due to compression is also unlikely to be found in real cases for the other casing strings in the well. For large size pipes, the load will cross the horizontal ellipse before crossing the API compression limit. For smaller sizes, due to the location of those casings in the wells, the loads that they will encounter cannot generate enough axial force to create failure in compression. This is therefore a regime that is not of much interest. Besides, buckling evaluation will be the leading one when compression load exists.

The well and cases evaluated in this example show that the use of the horizontal ellipse and the color scheme to present the tubular evaluation is very convenient as it presents clear information of which loads will lead to pipe failure and which will be the failure mode, avoiding misinterpretation of the information and helping engineers to choose the most suitable tubular for the well at the lowest cost.



# Chapter 5

## Conclusions

- The new API collapse equation presents advantages over previous formulations due to its reliance on the Von Mises triaxial theory that leads to calculations closer to test results. This is an important feature that can lead to reduce costs without sacrificing well integrity and could be especially relevant for HPHT projects that due to their high temperature and pressure require expensive tubular designs.
- A redefinition of the horizontal axis on the design limit plot occurs when superimposing the new API formulation for collapse on the ellipse of plasticity. A consequence of this change is a difficulty in plotting the API tension and compression limits. This disqualifies the commonly given justification to use the ellipse. With the current industry practice, the API limits cannot be plotted either in the circle of plasticity or in the ellipse.
- A relation between the ellipse and the circle of plasticity has been developed in the form of a horizontal ellipse and mathematically described by equations 4.7 and 4.8. This new relation is supported by industry publication results.
- As the most recent API collapse equation and the horizontal ellipse are based on the same theory, their plots are now compatible. Equation 4.10 is a brand new formulation that relates the horizontal ellipse with the new API triaxial collapse limit.
- The representation of the neutral equilibrium by two slanted lines in the original slanted ellipse is inconvenient as these lines look strange and unappealing. There is no visual agreement with the slanted direction of the ellipse and the direction of the neutral equilibrium lines. On the other hand, the use of a

vertical line located over the ordinate in the horizontal ellipse makes it easier to identify the stable and unstable regions.

- The proposed methodology to superimpose the API uniaxial limits in the slanted and horizontal ellipses using a color scheme has proven to work well and be convenient for all load cases, presenting clear information about unsafe loads and failure mode even if multiple cases are presented simultaneously.
- The results obtained from the industry-standard slanted ellipse and the one used by Goodman are in agreement with those obtained from the horizontal ellipse. This is reasonable since all models are based on the same underlying theory. A difference is that the tilted ellipse is based on zero axial stress datum while the horizontal ellipse/circle uses neutral axial stress datum.
- The horizontal ellipse is well suited for calculations involving buckling, is compatible with the information used in field operations, and, for being symmetric, its formulation is less complicated than the one of the slanted ellipse. These benefits call the attention to the horizontal ellipse, which model can be implemented to give the same results as the current industry software slanted ellipse model.
- For the "plastic" and "transition" collapse regimes experimental data are well correlated by the API triaxial collapse curve. For the "yield" collapse regime, the API equation is conservative.
- The API collapse equations are based on minimum statistical values and therefore the yield strength is a theoretical number. The relation between real values and this theoretical number defines the equation limit line in the design limits plot.
- An interesting future project is to include inclined and horizontal wells in the analysis of the horizontal ellipse using the color scheme methodology.

# Bibliography

- Aasen, J. A., & Aadnøy, B. S. (2003, January 1). Fully three-dimensional well design improves margins in critical wells [Journal Abbreviation: SPE-85302-MS], In *SPE-85302-MS*. SPE/IADC Middle East Drilling Technology Conference and Exhibition, SPE, Society of Petroleum Engineers. Journal Abbreviation: SPE-85302-MS. <https://doi.org/10.2118/85302-MS>
- Aasen, J. A., Ostvold, T. D., & Aadnoy, B. S. (2017, November 13). Revitalized three-dimensional design method improves tubular design [Journal Abbreviation: SPE-188605-MS], In *SPE-188605-MS*. Abu Dhabi International Petroleum Exhibition & Conference, Abu Dhabi, UAE, Society of Petroleum Engineers. Journal Abbreviation: SPE-188605-MS. <https://doi.org/10.2118/188605-MS>
- Aasen, J. A. (2007). *Buckling in oil and gas wells* (Doctoral dissertation) [ISBN: 9788276443295 Volume: no. 39]. University of Stavanger, Faculty of Science and Technology, Department of Petroleum Engineering. Stavanger. ISBN: 9788276443295 Volume: no. 39.
- Adams, A. J., Grundy, K. C., Kelly, C. M., Lin, B., & Moore, P. W. (2018, March 6). The barlow equation for tubular burst: A muddled history [Journal Abbreviation: SPE-189681-MS], In *SPE-189681-MS*. IADC/SPE Drilling Conference and Exhibition, SPE, Society of Petroleum Engineers. Journal Abbreviation: SPE-189681-MS. <https://doi.org/10.2118/189681-MS>
- API. (1989). *Bulletin on formulas and calculations for casing, tubing, drill pipe and line pipe properties* (5. ed., Vol. 5C3). Washington, API.
- API. (2015). *Technical report on equations and calculations or casing, tubing, and line pipe used as casing or tubing, and performance properties tables for casing and tubing : ANSI/API technical report 5c3 first edition, december 2008 : Addendum october 2015* (API TR 5C3, 1st edition). American Petroleum Institute. Washington, D.C.
- API. (2018). *Calculating performance properties of pipe used as casing or tubing* (API TR 5C3, 7th edition). American Petroleum Institute. Washinton, D.C.

- Belayneh, M. A. (2019). Grading, tube stress and failure analysis. University of Stavanger.
- Bellarby, J. (2009). *Well completion design* (Vol. vol. 56). Oxford, Elsevier.
- Byrom, T. G. (2007). *Casing and liners for drilling and completion* [ISSN: 9780128005705]. Houston, Texas, Gulf Pub.
- Clinedinst, W. O. (1980, December 1). *Calculating collapse resistance under axial stress using existing API collapse formulas and the strain energy of distortion theory of yielding* (Report prepared for the API). Dallas, Texas.
- Clinedinst, W. O. (1981, January 5). *Task group on performance properties of casing, tubing and drill pipe*. (Report of meeting). Bal Harbour, Florida.
- Goodman, M. A., Kalil, I. A., McSpadden, A. R., & Coker, O. D. (2017, April 5). New tubular design ellipse with backup pressure [Journal Abbreviation: SPE-185941-MS], In *SPE-185941-MS*. SPE Bergen One Day Seminar, SPE, Society of Petroleum Engineers. Journal Abbreviation: SPE-185941-MS. <https://doi.org/10.2118/185941-MS>
- Holmquist, J., & Nadai, A. (1939, January 1). A theoretical and experimental approach to the problem of collapse of deep-well casing [Journal Abbreviation: API-39-392], In *API-39-392*. Drilling and Production Practice, API, American Petroleum Institute. Journal Abbreviation: API-39-392. <https://doi.org/>
- Humphreys, A. T. (2000, January 1). Completion of large-bore high pressure/high temperature wells: Design and experience [Journal Abbreviation: OTC-12120-MS], In *OTC-12120-MS*. Offshore Technology Conference, Houston, Texas, Offshore Technology Conference. Journal Abbreviation: OTC-12120-MS. <https://doi.org/10.4043/12120-MS>
- Klever, F., & Tamano, T. (2004, January 1). A new OCTG strength equation for collapse under combined loads [Journal Abbreviation: SPE-90904-MS], In *SPE-90904-MS*. SPE Annual Technical Conference and Exhibition, SPE, Society of Petroleum Engineers. Journal Abbreviation: SPE-90904-MS. <https://doi.org/10.2118/90904-MS>
- Klinkenberg, A. (1951, January 1). The neutral zones in drill pipe and casing and their significance in relation to buckling and collapse [Journal Abbreviation: API-51-064], In *API-51-064*. Drilling and Production Practice, API, American Petroleum Institute. Journal Abbreviation: API-51-064. <https://doi.org/>
- Lubinski, A. (1975). Influence of neutral axial stress on yield and collapse of pipe. *Journal of Engineering for Industry*, 97(2), 400–407. <https://doi.org/10.1115/1.3438599>
- McSpadden, A., & Newman, K. (2002, January 1). Modified CT limits analysis for practical well intervention design [Journal Abbreviation: SPE-74828-MS], In *SPE-74828-MS*. SPE/ICoTA Coiled Tubing Conference and Exhibition,

- SPE, Society of Petroleum Engineers. Journal Abbreviation: SPE-74828-MS.  
<https://doi.org/10.2118/74828-MS>
- Mitchell, R. F., Lake, L. W., & Society of Petroleum Engineers. (2006). *Petroleum engineering handbook : Vol. 2 : Drilling engineering* (Vol. Vol. 2). Richardson, Tex, Society of Petroleum Engineers.
- Mitchell, R. F., Miska, S., Aadnøy, B. S., & of Petroleum Engineers (U.S.), S. (Eds.). (2011). *Fundamentals of drilling engineering* [OCLC: ocn711880603]. Richardson, TX, Society of Petroleum Engineers.
- Pattillo, P. D. (1985a). How to apply the new API adjustment for collapse resistance of tubulars. *Petroleum Engineer International*, 58.
- Pattillo, P. D. (1985b). How to apply the new API axial load adjustment. *Petroleum Engineer International*, 57.
- Ramsey, M. (n.d.). Casing. In *Schlumberger oilfield glossary*. Retrieved April 15, 2020, from <https://www.glossary.oilfield.slb.com/en/Terms/c/casing.aspx>
- Sparks, C. P. (1984). The influence of tension, pressure and weight on pipe and riser deformations and stresses. *Journal of Energy Resources Technology*, 106(1), 46–54. <https://doi.org/10.1115/1.3231023>
- Windenburg, D. F., & Trilling, C. (1934). Collapse by instability of thin cylindrical shells under external pressure. *Trans. Asme*, 11, 819–825.

# Appendix A

## Equation limit line

The data from collapse tests performed by a company and presented by Clinedinst to the API in 1980 (Clinedinst, 1981, Appendix 2022-1) are plotted in figures A.1 to A.11. The plots are presented using  $(\sigma_a + p_b)/Y$  in the abscissa and  $p/p_o$  in the ordinate. As explained by Clidenlinst: "This normalization is necessary since the API collapse values are on a statistical minimum basis while the Nippon Steel test are from pipe having tensile properties considerably above the API minimum values" Clinedinst, 1980.

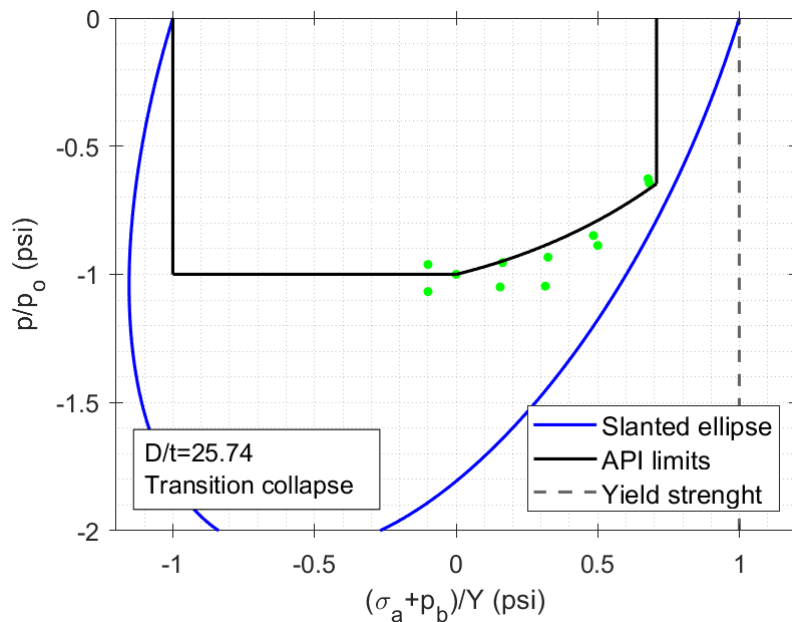


Figure A.1: Test data vs. API collapse limit for 7 in, 20 lb/ft, K55 pipe.

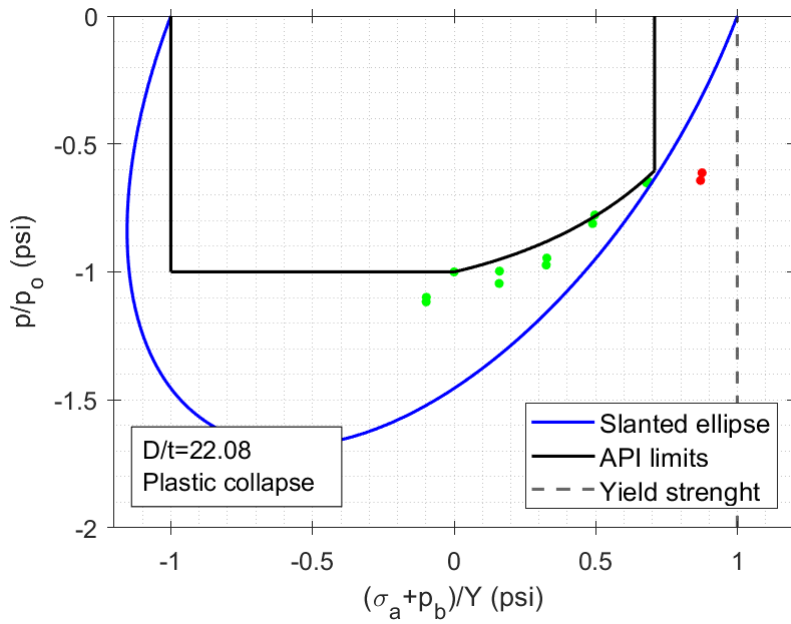


Figure A.2: Test data vs. API collapse limit for 7 in, 23 lb/ft, K55 pipe.

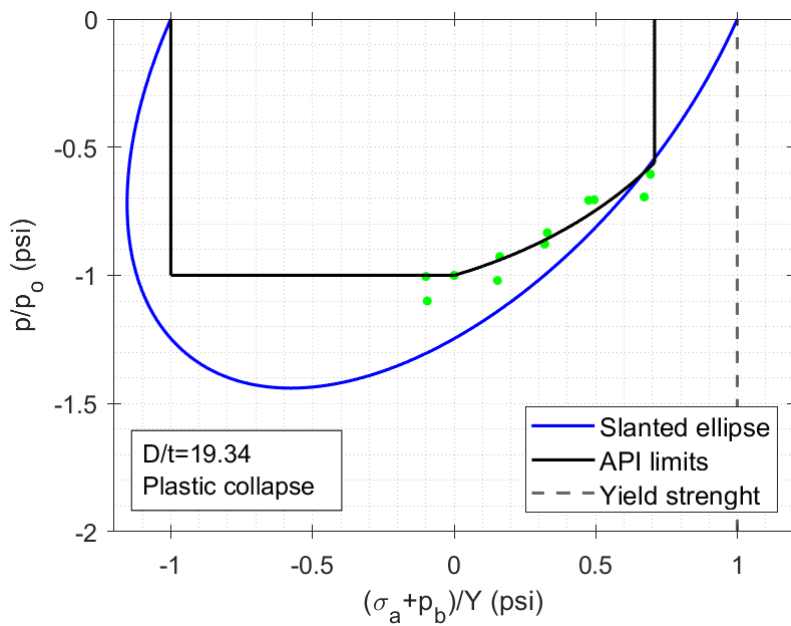


Figure A.3: Test data vs. API collapse limit for 7 in, 26 lb/ft, K55 pipe.

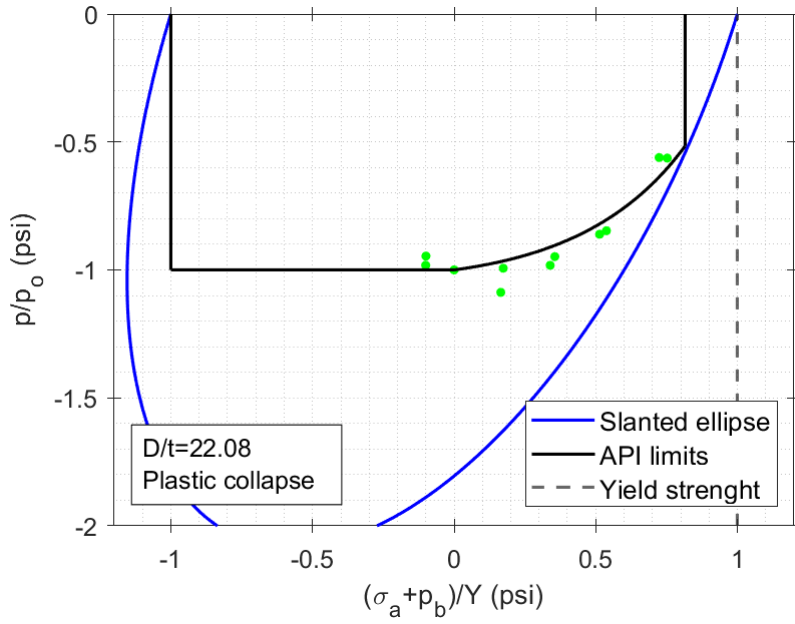


Figure A.4: Test data vs. API collapse limit for 7 in, 23 lb/ft, N80 pipe.

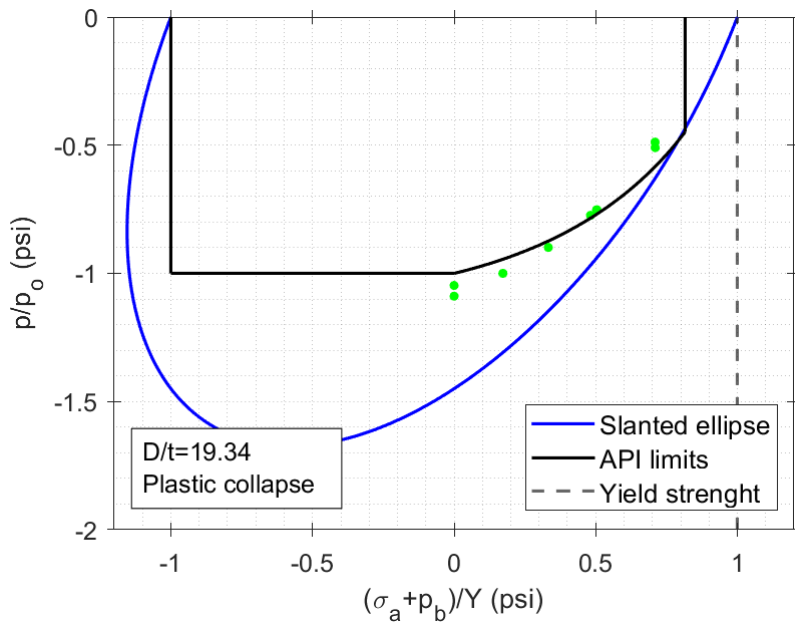


Figure A.5: Test data vs. API collapse limit for 7 in, 26 lb/ft, N80 pipe.



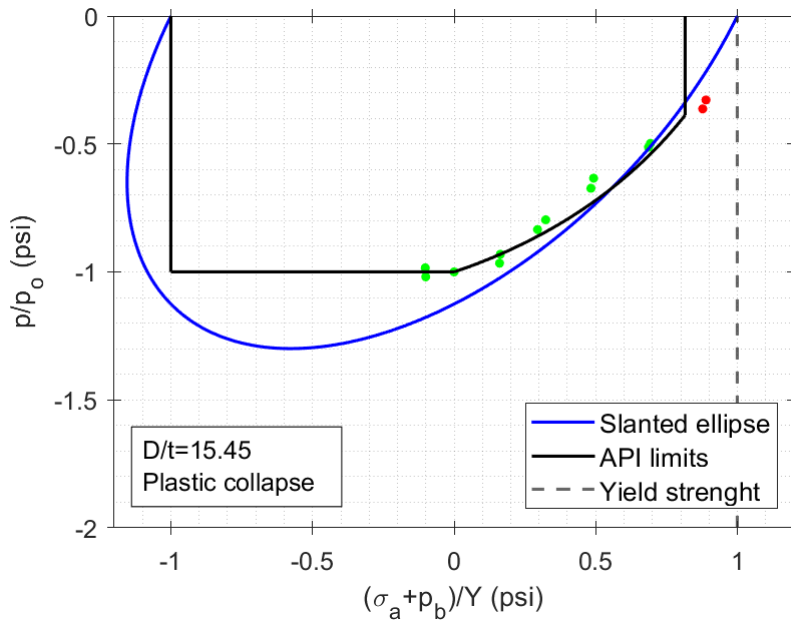


Figure A.6: Test data vs. API collapse limit for 7 in, 32 lb/ft, N80 pipe.

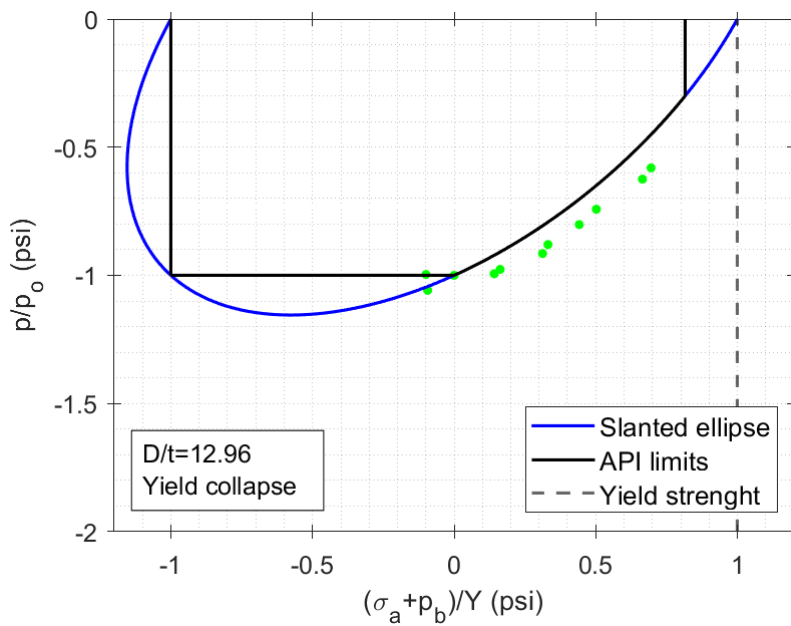


Figure A.7: Test data vs. API collapse limit for 7 in, 38 lb/ft, N80 pipe.

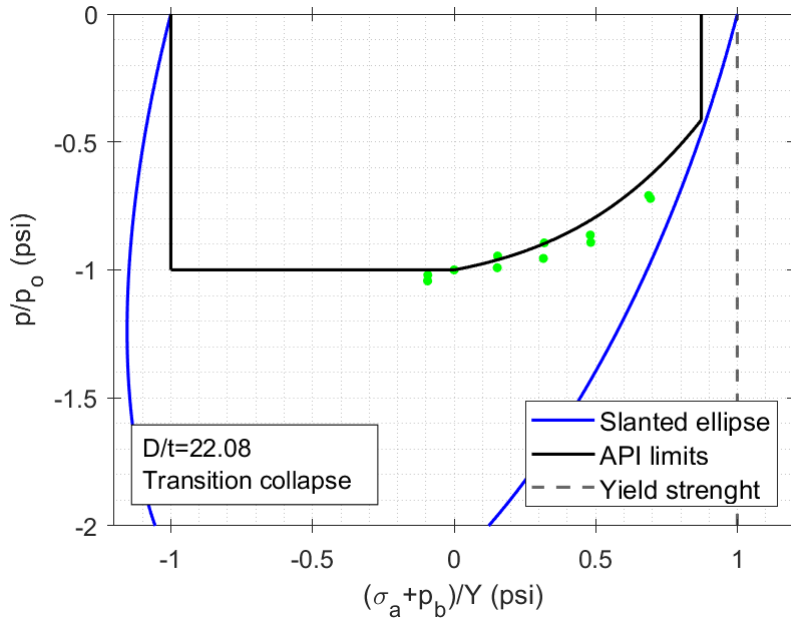


Figure A.8: Test data vs. API collapse limit for 7 in, 23 lb/ft, P110 pipe.

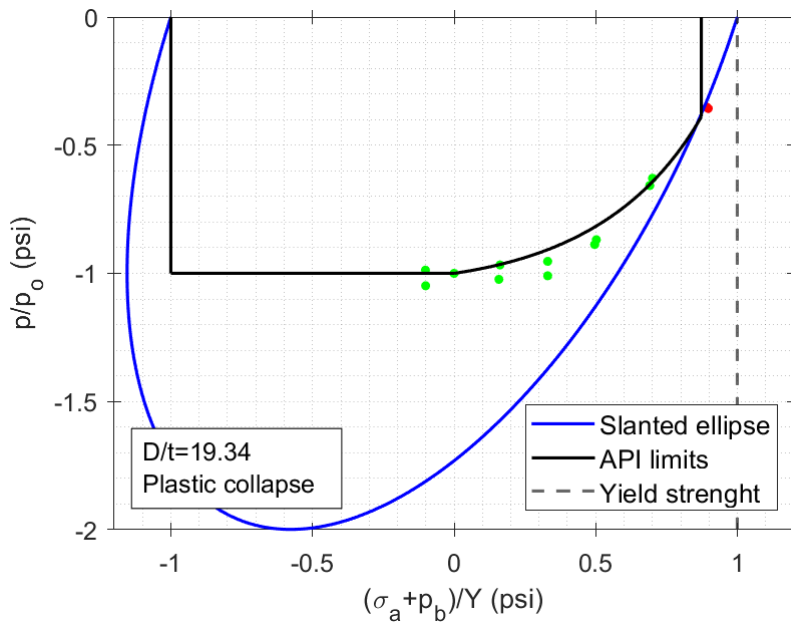


Figure A.9: Test data vs. API collapse limit for 7 in, 26 lb/ft, P110 pipe.

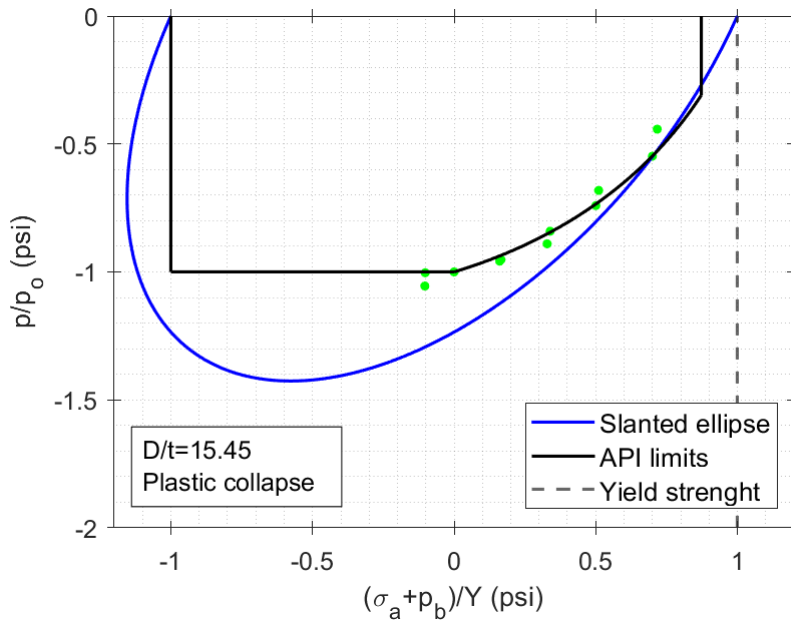


Figure A.10: Test data vs. API collapse limit for 7 in, 32 lb/ft, P110 pipe.

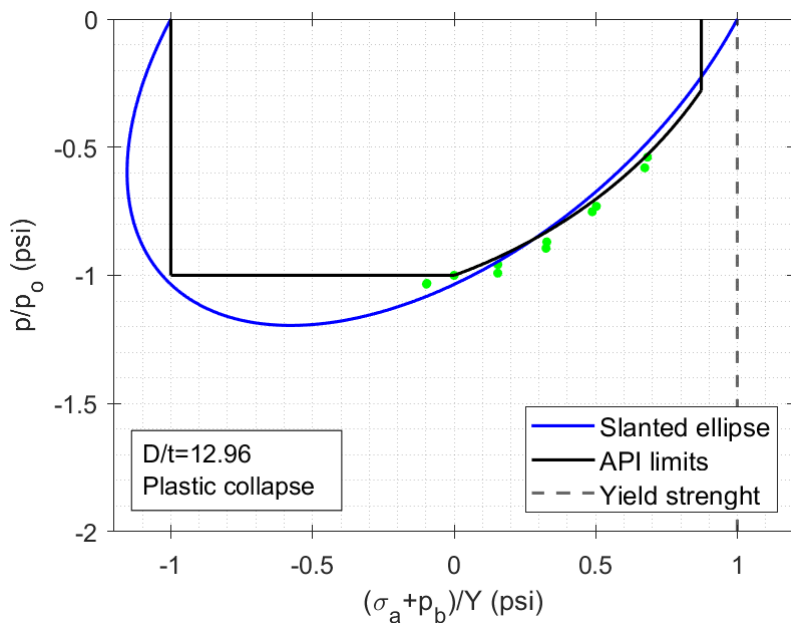


Figure A.11: Test data vs. API collapse limit for 7 in, 38 lb/ft, P110 pipe.

Most of the pipes fall in the "plastic" or "transition" regimes of collapse, as expected according to the theory presented in Chapter 2. The data is well correlated by the API formulation in both regimes. As the diameter of the pipe is reduced (and the  $D/t$  ratio is reduced) the collapse pressure increases and the API curve tends to get closer to the ellipse of plasticity. It is, however, overlapped only when the pipe falls in "yield" collapse. In this regime the API equation shows a more conservative result.

The 7 in, 23 lb/ft, K55; 7 in 32 lb/ft, N80; and 7 in 26 lb/ft P110 pipes are the only ones that present points outside the 24000 psi limit and which are to the left of the yield strength line. When looking at the data, those points have values of axial stress higher than the theoretical yield strength of the pipe and therefore are presented in red. When the same plots are presented without the use of the normalization proposed by Clidenlinst, this means using  $(\sigma_a + p_b)$  in the abscissa and  $\Delta p$  in the ordinate (the data considers only axial load, therefore  $\Delta p$  is the collapse pressure) figures A.12 to A.14 are obtained.

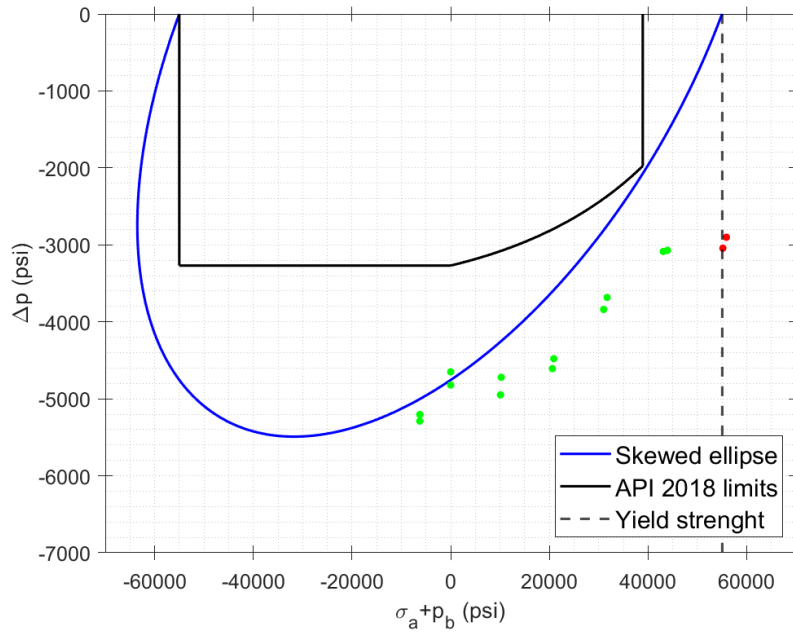


Figure A.12: Collapse ellipse for 7 in, 23 lb/ft, K55 pipe.

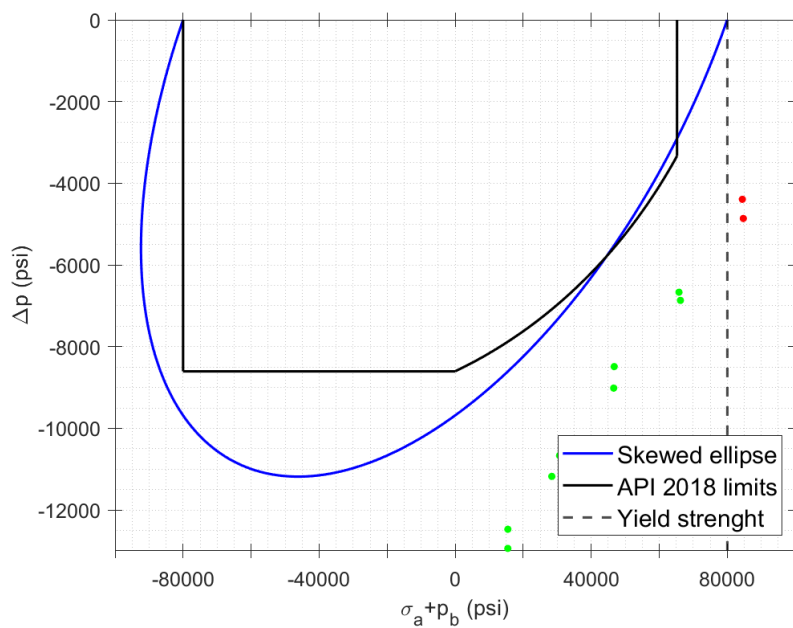


Figure A.13: Collapse ellipse for 7 in, 32 lb/ft, N80 pipe.

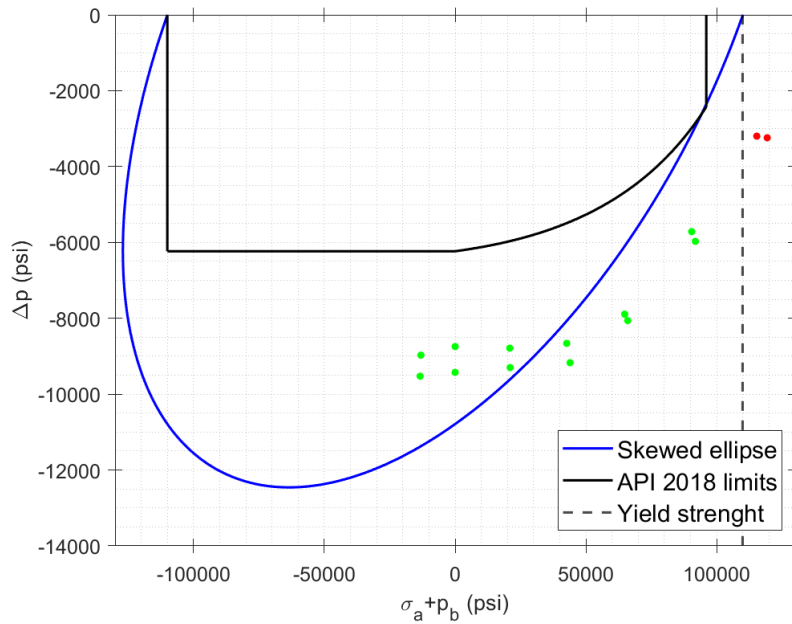


Figure A.14: Collapse ellipse for 7 in, 26 lb/ft, P110 pipe.

The red loads that appear to the right of the equation limit line in the normalized plot (figures A.2, A.6 and A.9) are to the right of the yield strength in the regular scale plots (figures A.12 to A.14). The API equations are statistically adjusted to calculate minimum collapse values in order to ensure safe designs (Pattillo, 1985b) and the yield strength given by the pipe grade is a theoretical number that has a higher value than in the real data. The equations limit line accounts for the difference between the minimal values and the real mechanical properties of a pipe and is therefore a requirement of the normalized plots to make sure that unsafe loads are outside the API limits. This project is based in the use of API equations and theoretical properties and the results are presented using the regular plots, therefore, the limit can be disregarded and be plotted as a straight line that connects the collapse pressure curve with the value of the yield strength on the horizontal axis.

# Appendix B

## Derivation of equation 4.8

Starting from equations 2.14 and 2.15:

$$\Delta\sigma_a = \sigma_a - \sigma_n = \sigma_a - \frac{d^2 p_i - D^2 p_o}{D^2 - d^2}$$

In the case of burst, the back up pressure corresponds to the outside pressure. Adding and subtracting it:

$$\Delta\sigma_a = \sigma_a - \frac{d^2 p_i - D^2 p_o}{D^2 - d^2} + p_o - p_o$$

$$\Delta\sigma_a = (\sigma_a + p_o) - \frac{d^2 p_i - D^2 p_o}{D^2 - d^2} - p_o$$

$$\Delta\sigma_a = (\sigma_a + p_o) - \frac{d^2 p_i}{D^2 - d^2} + \frac{D^2 p_o}{D^2 - d^2} - p_o \frac{(D^2 - d^2)}{(D^2 - d^2)}$$

$$\Delta\sigma_a = (\sigma_a + p_o) - \frac{d^2 p_i}{D^2 - d^2} + \frac{p_o}{D^2 - d^2} (D^2 - D^2 + d^2)$$

$$\Delta\sigma_a = (\sigma_a + p_o) - \frac{d^2}{D^2 - d^2} (p_i - p_o)$$

Multiplying by  $D^2/D^2$  on the right side:

$$\Delta\sigma_a = (\sigma_a + p_o) - \frac{d^2}{D^2} \frac{D^2}{D^2 - d^2} (p_i - p_o)$$

Using the definitions of  $k$  and  $\beta$  from equations 2.24 and 2.19 respectively:

$$\Delta\sigma_a = (\sigma_a + p_o) - \frac{1}{2}k\beta(p_i - p_o)$$

This is the equation that relates the circle with the ellipse of plasticity for the burst half of the plot.